I S T C
М Н Т Ц

НИИ НПО "ЛУЧ"

PROJECT # 3194

"Fuel assembly tests under severe accident conditions"

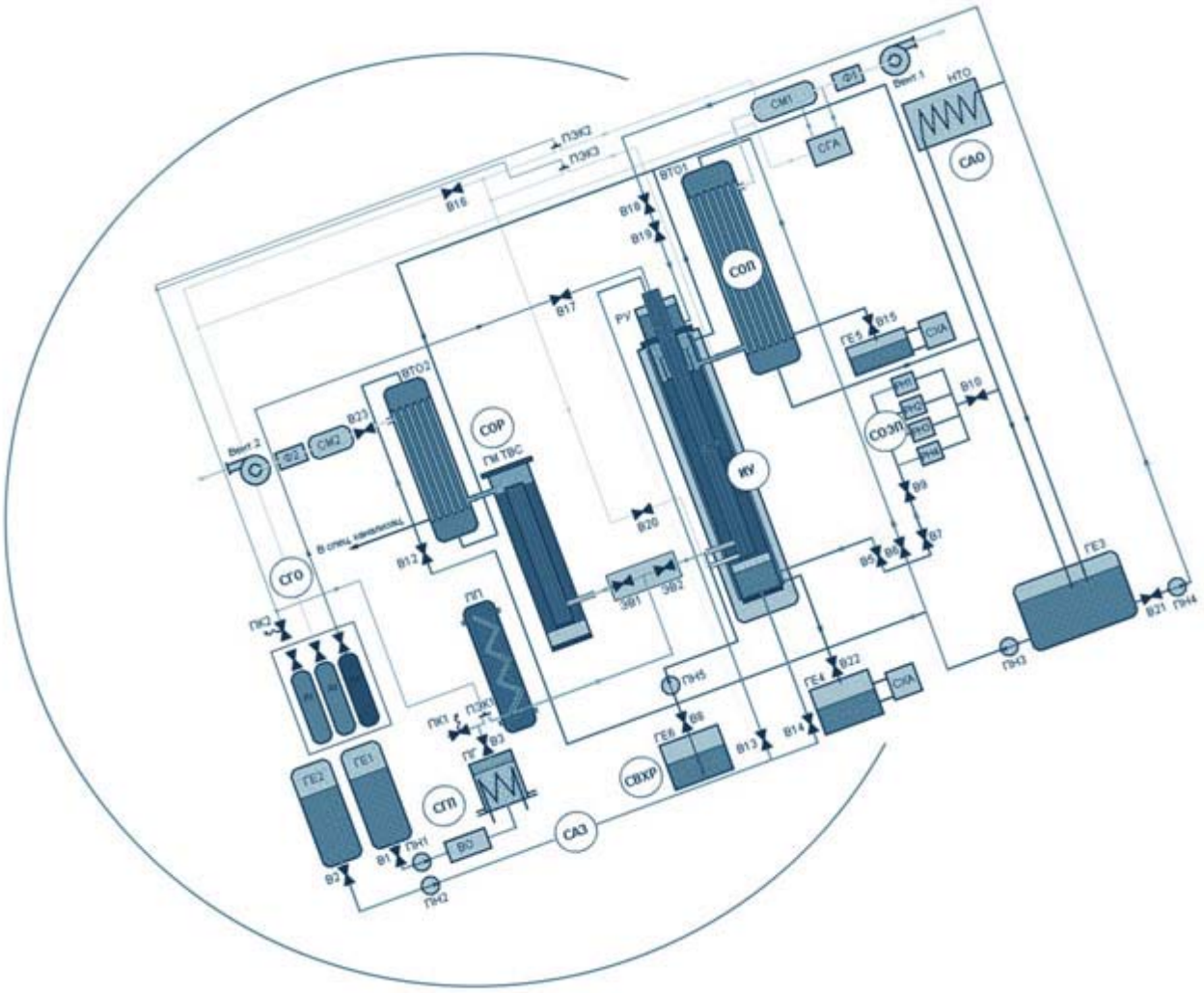

2007

PROTOCOL

on the results of the model FA
material studies
after the PARAMETER-SF1 experiment

2007

INTRODUCTION

According to the Work Plan for ISTC Project # 3194, the dismantling, preservation, partition and post-test material studies of the model FA of VVER-1000 were performed after the PARAMETER-SF1 experiment in FSUE SRI SIA “LUCH” during May-November 2006. The studies were conducted together with IBRAE RAS, A.A. Botchvar FSUE VNIINM, with the methodical support of foreign collaborators (FZK).

The purposes of the material studies were:

- Description of the post-test state of the model FA VVER-1000 and analysis of its components (degree of oxidization, structure, chemical and phase compositions);
- Evaluation of distribution of the flow area blockage, transfer of the melt and thinning of fuel pellets over the assembly height.

1. Methods of preservation, partition and material studies of the model FA after the tests

Preservation of the model FA after the PARAMETER-SF1 experiment was performed in vertical position by means of filling the thermal insulation housing with epoxy resin ЭД-20 without partition. Such solution was taken to minimize damages in FA (crumbling) during post-test procedures.

On solidifying the epoxy resin the thermal insulation housing of the horizontally positioned model FA was uncovered (Fig. 1) and thermal insulation was removed mechanically. The external appearance of the model FA after removal of thermal insulation is presented in Fig. 2.

The transverse cuts were made with the use of cutting-off machine Delta-Abrasimet with diamond wheel of thickness 1.3 mm. The exact values of coordinates of the transverse cuts are presented in Table 1.

To remove voids and cavities remained after FA filling the specimens vacuum impregnation was made with epoxy resin EPO – THIN at the “Buehler” impregnator. Then the templets, chosen for metallographic examination, have been ground and polished.

The macro photos of the ground templets were taken by the digital camera SONY (8 mps). Further on the obtained views were used for digital processing and obtaining the dependences of the melt distribution, the flow area blockage and the fuel dissolution over the FA height. *The flow area blockage (COB) was determined by the formula:*

$COB = (S_{изм}-S_{тв})/(S_{ч}-S_{тв})\cdot 100\%$, where

$S_{изм}$ – the measured area of material;

$S_{тв}$ – the initial cross-section area of 19 fuel rods (1242 mm^2);

Sч – the initial cross-section area of the shroud (2820 mm^2).

Degree of the fuel dissolution with the melt was determined by the relationship:

UO_2 ост.= 100 - (So-Sизм)/So·100%, where

Sизм – the measured area of UO_2;

So – the initial cross-section area of fuel rod pellets (576 mm^2).

Metallographic analysis of templets was performed at the optical microscope OLYMPUS using the programme package OMNIMET. Electron-microscopic studies and EDX analysis of the templets were performed at the scanning electron microscope JEOL JSM – 6460 LV with the use of energy dispersion adapter OXFORD. Radiographic phase analysis of fuel fragments and melt droplets was conducted after mechanical withdrawal from templets. To eliminate the effect of the melt structural features (coarse grain, grain orientation) on the analysis results the withdrawn fragments were reduced to powder and then subject to radiography. Phase analysis was conducted at the diffractometer DRON-6 with the use of CuKα – radiation.

2. Results of material studies

2.1. Description of FA external appearance

Visual examination of the thermal insulation housing (stainless steel cylinder with thickness of 1 mm) after withdrawal of the assembly from the working section showed presence of blowhole (Fig. 3) at the level of $\sim$ 800 mm on the assembly face 90^o – 120^o (fuel rods 3.7 – 3.9).

On the housing inner surface (Fig. 1) and on the thermal insulation outer surface (Fig. 4) the local oxidized areas with peeling oxide scum and solidified melt were revealed.

In Fig. 2 the external appearance of the model FA is given with the shroud at the level of 700 – 1000 mm on the assembly face 90^o – 120^o (fuel rods 3.7 – 3.9) after thee experiment. The shroud is swelled, strongly oxidized and partially damaged.

In Fig. 5-7 the photos of templets are given (top view). Fuel rod 3.1 is marked for orientation.

2.2. Analysis of the cross-section structures

2.2.1. Elevation range 402 – 582 mm

At the level of Z = 402 mm there are practically no visible damages of the assembly (Fig. 8). Maximum temperature at this level did not exceed 900°C by indications of thermocouples. Some pellets of uranium dioxide have cracks. In some pellets there are no fuel fragments. However crumbling of pellets is not related to fuel damage during the

experiment and it rather occurred in the course of the assembly cutting or preparing the section metallographic specimen.

Microstructure of material of fuel rod simulator claddings, housing, fuel pellets does not practically differ from the structure of material before performing the experiment. Thickness of oxide layer on the cladding outer surface is ~ 6 μm, no internal oxidization of claddings was revealed, except for the central rod cladding. Hexahedral cladding was oxidized both from the inside, and outside, with this, the thickness of oxide layer of the shroud corresponds to the thickness of oxide layer of claddings (~ 6 μm (Fig.9)).

At the level of Z = 536 mm the assembly looks like undamaged as before (Fig. 10). The saved spacing grid is clearly seen. The fuel rod claddings are oxidized from the outside, the shroud is oxidized both from the outside, and inside. Thickness of their oxide layer is ~ 8 μm (Fig.11). No areas of fuel-clad interaction is revealed, that is in agreement with indications of thermocouples (maximum registered temperature at the given level did not exceed 1000°C).

In gaps between fuel rods (in the spacing grid cells) two droplets of the melt were revealed (Fig. 10). The droplets are not in contact with the FA structural components. No specific features in microstructure of claddings and spacing grids, located near droplets of the melt, were revealed. Thus, a conclusion can be made that this level is reached by small, relatively cold portions of the melt that solidified quickly not causing even local heating-up that could lead to different physical-and-chemical interactions. Structures of the melts are presented in Fig.12. Metallographic analysis showed that the structure of the melts is a metal matrix with ceramic precipitates nonuniformly distributed over the melt section. Electron-microscopic and EDX analysis of the melts showed that the studied droplets represent a metal melt of (U,Zr,O) type (grey phase) wherein ceramic precipitates (bright and dark phases) were formed. Chemical composition of the melts and their compounds is presented in Table 2. Thickness of oxide phase on the surface of droplets does not exceed 10 μm.

There was a small change in the assembly configuration at the level of Z = 582 mm. In the same places the solidified droplets of the melt of larger area were revealed that is indicative of the melt running down at this level in the form of steams. Besides, the melt was revealed between the cladding and fuel pellet of presence of fuel rod 3.9. No layers, typical for eutectic fuel-clad interaction were revealed, that is in agreement with indications of thermocouples (temperature in this area did not exceed 1000°C as per the indications of thermocouples). Presence of the melt between the cladding and fuel can be evidently explained by entering of the melt from above through a gap between the cladding and the pellet.

At the given level the EDX analysis was performed for the melts in the space between fuel rods (Table 3). Then fragments of these melts were withdrawn mechanically from the templet and transferred for conducting the radiographic phase analysis.

Results of the radiographic phase analysis showed that in the melt the main phase is the metal phase – the solid solution of oxygen in alpha zirconium (α - Zr(O)). Analysis of periods of the solid solution grid α - Zr(O) showed that it is saturated in oxygen at the maximum (~30 at%). Alongside with the metal phase there are also ceramic phases $(U,Zr)O_2$, $(Zr,U)O_2$ and Zr_6Fe_3O in the melt. Phase composition of the melt in the center and on the periphery of the assembly does not principally differ.

2.2.2. Elevation range 652 - 699 mm

At the level of Z = 652 mm the displacement of the fuel rod central cladding was observed as well as considerable accumulation of the melt in the space between fuel rods, between the shroud and fuel rods (Fig.13).

The solidified melt was revealed in the gap between fuel pellets of UO_2 and claddings, run down through the internal voids of fuel rods (fuel rods 2.4, 2.5, 2.6, 3.1, 3.6, 3.8, 3.9) and dissolving the metal part of claddings (fuel rod 3.8., Fig. 14, thickness of the cladding is ~ 500 μm, thickness of the melt is ~ 200 μm, thickness of α - Zr(O) + (U,Zr) layer is ~ 20 μm). The traces of fuel-clad interaction of fuel rods 2.1, 2.2, 3.2, 3.4, 3.7 and 3.9 (Fig.14, fuel rod 3.4) were revealed as well. It follows from the metallographic analysis of the interaction zones and the character of location of cladding and pellets in respect to each other that it resulted from the fuel-clad interaction under their local contact caused by misalignment of claddings and fuel (Fig.14, fuel rod 3.4, thickness of α - Zr(O) + (U,Zr) layer is ~ 10 μm, thickness of (U,Zr) layer is ~ 20 μm).

The hot melt running down the outer surface of fuel rods made a considerable contribution into heating of fuel rods and, as a consequence, resulted in intensification of the fuel-clad interaction processes.

Structures of the melts from the space between fuel rods and the results of EDX analysis are presented in Fig. 15 and in Table 4. Formation of cracks in the solidified melt is indicative of its brittleness due to increased content of the dissolved oxygen. Thickness of oxide phase on the melt surface does not exceed 50 μm. The eutectic interaction of thermocouple housings (stainless steel) with the fuel rod cladding (fuel rod 3.6) was revealed.

In spite of considerable changes the most part of fuel rod claddings kept their integrity at the given level. Thickness of oxide scum on the outer surface of claddings does

not exceed ~ 20 μm, on the inner surface of some claddings it is 2…3 μm. In the places of the contact with hot melt, run from the top, a part of claddings is dissolved to a different extent (fuel rods 2.5, 3.2, 3.7, 3.8, 3.9, 3.10). Oxidization of the shroud on the outer surface (oxide thickness is ~ 30…100 μm) took place considerably stronger than on the inner surface (oxide thickness is ~ 5…10 μm).

At the level of Z = 679 mm (top view) the amount of the melt in the space between fuel rods increased, some fuel rod claddings were damaged significantly and lost their integrity. Sufficiently higher number of fuel rod claddings interacted with fuel pellets. Structure of zones of the eutectic interaction and melt in gaps is indicative of the fact that:

- in a part of fuel rods there was again the fuel-clad interaction locally in the places of contact (fuel rods 2.1, 2.2, 3.5 *и* 3.7),

- in fuel rods 2.3 – 2.6, 3.1, 3.3, 3.8, 3.9 and 3.10 there was interaction of claddings and fuel with the melt.

In some zones the melt, running from above, made evidently the local heating of cladding to high temperature in such a way that the metal part of claddings was melted. Liquid zirconium dissolved fuel and oxide part of claddings.

Results of integral EDX analysis are presented in Table 5. Phase composition of the melt at the given level is similar to section Z = 582 mm. The eutectic interaction of thermocouple jackets (stainless steel) with fuel rod cladding was revealed that is similar to Z = 652 mm (Fig.17, fuel rod 3.6). Damage of fuel rod claddings at the places of contact with the melt was governed by local heating of claddings to temperature of 1870°C due to the heat entrained with the hot melt and subsequent two-sided dissolution. No facts were revealed that confirm melting of metal zirconium in claddings not contacting the melt.

In cross-section Z = 699 mm the considerable damage was revealed of not only the fuel rod claddings, but also of the FA shroud (Fig.18), that evidently is indicative of reaching the melting temperature of metal zirconium at the given level (~1870°C). The shape of fuel rod claddings was kept owing to the outer high-melting oxide part. Thickness of zirconium dioxide does not exceed ~170 μm. In places of contact with the melt the claddings are damaged to higher extent. The cladding damage resulted in outflowing of the melt to thermal insulation. Formation of cracks in the solidified melt is indicative of its brittleness that corresponds to the increased content of oxygen (Fig.19). Oxide thickness on the outer surface of the shroud does not exceed ~ 200 μm, and ~ 60 μm – on the inner surface.

Study of cross-sections of fuel rods shows the structure typical for dissolution of cladding and fuel with the melt and for outside oxidization (Fig. 20). The structure and

composition of the melt are presented in Figs. 20, 21, 22 and in Table 6. Thickness of oxide phase on the melt surface does not exceed ~300 μm.

2.2.3. Elevation range 724 - 793 mm

Within the elevation range of Z = 724…793 mm the geometry of fuel rods arrangement in the assembly is kept although the FA shroud and fuel rod claddings are absent completely. Some fuel pellets are fragmented. The melted and run down masses made blockage of the FA flow area practically completely (Fig. 23).

At the level of Z = 724 mm (top view) the melt filled almost the whole space between fuel rods. Results of EDX analysis of the melt are presented in Table 7, and typical structures are given in Fig. 25. The obtained data are indicative of relative uniformity of the ceramic phase in the melt due to which it can be supposed that its formation occurred at higher level. Thickness of oxide phase on the melt surface in the given section does not exceed 400 μm.

The specific feature of the zone with tight blockage is the fact that over the height it consists of two parts (at the level of Z = 724 mm and Z = 793 mm), between which (Z = 745 mm) there is no melt practically (Fig. 26), and fuel pellets are dissolved considerably (Fig. 27). On pellet surfaces the traces of melt with ceramic composition are revealed. Structures and results of EDX analysis of the melt are presented in Fig. 28 and in Table 8.

At the level of Z = 793 mm (Fig. 29) the melt is characterized by large nonuniformity through the section. The melt region, contacting the fuel rods, has metal luster, whereas the melt regions on the assembly periphery are of mat shade. Results of macroscopic studies (Fig. 30, 31) and EDX analysis, presented in Table 9, are indicative of the fact that the structure and composition of the mat melt correspond to the ceramic composition and similar to the melt revealed on the fuel surface at the level of Z = 745 mm. Thickness of oxide on the melt metal part reaches 800 μm.

Radiographic phase analysis showed that:

- in the central part of the given section there is the metal melt with the main phase of α - Zr(O) ultimately saturated with oxygen (Fig. 29, Zone A),

- on the periphery there are ceramic phases, in the main ($(Zr,U)O_2$ – the main phase and ZrO_2 of monowedge modification, Fig. 29, Zone Б).

2.2.4. Elevation range 839 - 1066 mm

The assembly state within the elevation range of Z = 839 - 1066 mm (Fig. 32, 34, 36, 38, 42) is characterized by complete absence of zirconium structural components (FA

shroud, fuel rod claddings, spacing grids, thermocouples jackets) that is indicative of the level of temperatures considerably exceeding the zirconium melting temperature within the given elevation range. Apparently, the melt, formed within this elevation range, caused the considerable blockage below. Integrity of the remaining fuel columns is kept only at the expense of tantalum heaters playing the role of the assembly skeleton that reflects adequately the behaviour of the full-scale FA under similar conditions. In some of the regions of each of the sections studied for the given elevation range the fragments were revealed of the through-oxidized fuel rod claddings, or the oxide scums peeled from the fuel rod claddings (Fig. 38, 40). Their presence could be also caused by transfer of brittle fragments from the upper levels (crumbling) of transfer from the low levels when filling the assembly with epoxy resin (lifting).

Cracking of fuel pellets is observed. Starting from the level of 1066 mm and higher, a part of pellets is fragmented. In the space between fuel rods their large fragments are identified, however no substantial transfer of the fuel is revealed due to crumbling of pellet fragments. It is necessary to not also that the diameter of fuel pellets reduced considerably due to dissolution of uranium dioxide with the melt that, apparently, run down on the surface of fuel columns (Fig. 33, 35, 37, 39, 41). Remains of the melt were revealed both on the outer surface of fuel pellets, and in the fuel-heater gap. Radiographic-structural analysis of the fuel pellet surface from the level of Z ~ 900 mm showed presence of ceramic phase $(Zr,U)O_2$. Analysis of the pellet itself showed that it consists of super stoichiometric uranium dioxide UO_{2+x}.

Tantalum exists in the composition of the melt between the fuel pellet and the heater. Typical structures of the given melt are presented in Fig. 46, results of EDX analysis – in Table 10.

2.2.5. Elevation range 1091 - 1263 mm

The upper part of the model FA (Z = 1091…1263 mm) kept its integrity though the assembly geometry is disturbed considerably. The shroud within this elevation range kept its shape owing to high-melting oxides on the outer and inner surfaces. At the level of Z = 1091 mm a part of fuel pellets is fragmented, in the space between fuel rods the large parts of fuel pellets can be seen. Around the intact fuel pellets the remains of claddings are identified. The intact parts are oxidized completely (Fig. 43, 45). The metal part of claddings at these levels was melted and partially run down into the assembly lower part, that is evident from the revealed voids between the remains of claddings and fuel. The remaining melt between claddings and fuel contains uranium, the fuel is partially dissolved.

Starting from this level, and moving to the assembly upper part, the smaller amount of damages is observed that is caused by quick water cooling under top flooding.

At the level of Z = 1263 mm (top view) the thickness of oxide scum on the outer surface of claddings is ~ 200 μm, the oxide is of columnar structure without laminations. With this, all fuel rods at the given level are intact but have the through cracks (Fig. 51) with the edges not oxidized that is indicative of the fact that they were formed under flooding. In claddings of fuel rods 3.12 and 3.6 the traces of eutectic fuel-clad interaction were revealed (Fig. 51, thickness of α - Zr(O) + (U,Zr) layer is ~ 100 μm, thickness of (U,Zr) layer is ~ 70 μm). Thickness of oxide on the shroud outer and inner surfaces is ~ 150 μm.

2.2. Assembly height distribution of the flow area blockage, transfer of the melt and thinning of fuel pellets

As a result of studies of the cross-sections the considerable dissolution of fuel pellets was revealed. For quantitative evaluation of the fuel dissolution in each section the area of each pellet was measures and using the above-mentioned procedure the dependence was plotted of the fuel dissolution over the FA height (Fig. 52).

Profile of the solidified melt in the assembly is presented in Fig. 53.

For calculation of the assembly flow area blockage in each cross-section the area of the whole material available was calculated, except for the shroud and remains of thermal insulation. Using the obtained result the change of the flow area in the assembly and COB were calculated. It should be noted that the blockage was calculated in respect to the initial flow area. In this connection the COB in section Z = 793 mm reaches 100% (Fig. 54), although visually (Fig. 29) it is seen that the flow area remains.

3. Conclusions

The state of the model FA of VVER-1000 after the PARAMETER-SF1 experiment differs significantly over the height, and in this connection its heated part was conventionally divided into five zones by the degree and character of damage (Fig. 55).

In the first zone (Z ~ 0…540 mm) there are no substantial damages of the assembly. Thickness of oxide on the surface of zirconium components does not exceed 10 μm.

In the second zone of the assembly (Z ~ 540…700 mm) there are solidified droplets and streams of the melt (U,Zr,O), moved from the assembly upper part. Starting from the level of 650 mm and above the zones of fuel-clad interaction are revealed. The hot melt, coming from the assembly upper levels, resulted in local temperature increase and, as a

consequence, in intensification of the running processes. At higher levels of this zone a partial melting of metal zirconium occurred, as well as fuel dissolution by the formed liquid mixture, the claddings were dissolved both from the outside, and inside. Thickness of oxide on the cladding surfaces in this zone increases from 10 to 170 μm with increase of height coordinate. The shroud is oxidized on both sides. With increase of height coordinate the thickness of oxide increases within the range of 10…80 μm and 10…200 μm on the inner and outer surfaces, respectively. On the melt surface there is the oxide layer with the thickness not exceeding ~300 μm. The melt structure is not uniform through the section. Its main phase is the metal phase α - Zr(O) (60-85%). The composition includes also the ceramic phases $(U,Zr)O_2$, $(Zr,U)O_2$ and Zr_6Fe_3O in the form of precipitates.

In the third zone (Z ~ 700…800 mm) the melted and rundown masses formed practically complete blockage of the FA flow area. The specific feature of the tight blockage zone is the fact that it comprises two parts over the height (this was revealed through sections at the levels of Z = 724 mm and Z = 793 mm), and between them (Z = 745 mm) there is no melt practically in the space between fuel rods and fuel pellets are considerably dissolved. The lower part of the blockage presents the metal melt with ceramic precipitates (20-40%), thickness of oxide on the melt surface does not exceed ~ 400 μm. The upper part of the blockage – the central zone – is the metal zone (content of precipitates is 30-60%, thickness of oxide on the surface is up to 800 μm), the periphery is the ceramic zone $(Zr,U)O_2$.

The fourth zone (Z ~ 800 – 1070 mm) is characterized by damage of zirconium structural components and considerable dissolution of fuel pellets, however no substantial masses of the melt were revealed. On the cladding surfaces there are traces of the melt of ceramic structure of the mixed composition $(Zr,U)O_2$.

In the fifth zone (Z ~ 1050 – 1250 mm) the remains of oxide parts of fuel rod claddings and melt were revealed, as well as remains of the shroud. Thickness of oxide of claddings at the level of ~ 1250 mm is ~ 200 μm. the shroud is oxidized on both sides, thickness of oxide on the outer and inner surfaces is ~ 150 μm. No facts confirming melting of metal zirconium at this level were revealed.

TABLES

Table 1. Coordinates of transverse cuts

Specimen	Specimen length, mm	Specimen coordinate		Remarks
		Bottom, mm	Top, mm	
Cut	1.3	385.4	386.7	
	15	386.7	401.7	templet
Cut	1.3	401.7	403	
	18	403	421	
Cut	1.3	421	422.3	
	59	422.3	481.3	
Cut	1.3	481.3	482.6	
	33	482.6	515.6	
Cut	1.3	515.6	516.9	
	19	516.9	535.9	templet
Cut	1.3	535.9	537.2	
	22.8	537.2	560	
Cut	1.3	560	561.3	
	21	561.3	582.3	templet
Cut	1.3	582.3	583.6	
	22.3	583.6	605.9	section metallographic specimen+radiography
Cut	1.3	605.9	607.2	
	19.9	607.2	627.1	
Cut	1.3	627.1	628.4	
	23.4	628.4	651.8	templet + radiography
Cut	1.3	651.8	653.1	
	25.4	653.1	678.5	templet
Cut	1.3	678.5	679.8	
	19.4	679.8	699.2	templet
Cut	1.3	699.2	700.5	
	23	700.5	723.5	section metallographic specimen+radiography
Cut	1.3	723.5	724.8	
	20.3	724.8	745.1	templet
Cut	1.3	745.1	746.4	

	23	746.4	769.4	section metallographic specimen+radiography
Cut	1.3	769.4	770.7	
	22.4	770.7	793.1	templet
Cut	1.3	793.1	794.4	
3.2	19.8	794.4	814.2	
Cut	1.3	814.2	815.5	
4.1	**23.6**	815.5	839.1	templet
Cut	1.3	839.1	840.4	
4.2	21.7	840.4	862.1	
Cut	1.3	862.1	863.4	
5.1	**22.5**	863.4	885.9	templet
Cut	1.3	885.9	887.2	
5.2	21.7	887.2	908.9	
Cut	1.3	908.9	910.2	
6.1	20	910.2	930.2	templet
Cut	1.3	930.2	931.5	
6.2	21.5	931.5	953	
Cut	1.3	953	954.3	
7.1	**21.5**	954.3	975.8	templet
Cut	1.3	975.8	977.1	
7.2	23.6	977.1	1000.7	
Cut	1.3	1000.7	1002	
8.1	19.6	1002	1021.6	templet
Cut	1.3	1021.6	1022.9	
8.2	22	1022.9	1044.9	
Cut	1.3	1044.9	1046.2	
9.1	**20**	1046.2	1066.2	templet
Cut	1.3	1066.2	1067.5	
9.2	**23.8**	1067.5	1091.3	templet
Cut	1.3	1091.3	1092.6	
10.1	22.7	1092.6	1115.3	
Cut	1.3	1115.3	1116.6	
10.2	22.7	1116.6	1139.3	
Cut	1.3	1139.3	1140.6	

	15.8	1140.6	1156.4	templet
Cut	1.3	1156.4	1157.7	
	19.4	1157.7	1177.1	
Cut	1.3	1177.1	1178.4	
	68.3	1178.4	1246.7	
Cut	1.3	1246.7	1248	
	15	1248	1263	templet
Cut	1.3	1263	1264.3	
	22	1264.3	1286.3	
Cut	1.3	1286.3	1287.6	

Table 2. Results of EDX analysis of the melt (Z = 536 mm)

Description of zone (Fig.10)	**Chemical composition, wt.%**						
	Zr	**U**	**Fe**	**Cr**	**Ni**	**O**	**Ta**
Droplet of melt No.1 (in total)	77.6	9.0	0.3	-	-	13.0	-
Bright phase	32.0	50.0	0.4	0.2	0.2	18.2	-
Grey phase	85.0	5.0	-	-	-	10.0	-
Dark phase	66.0	10.0	-	-	-	24.0	-
Droplet of melt No.2 (in total)	77.7	0.6	0.4	-	-	12.3	-
Bright phase	39.9	46.5	0.9	0.2	0.3	19.2	-
Grey phase	85.7	3.9	-	-	-	10.4	-

Table 3. Results of EDX analysis of the melt (Z = 582 mm)

Description of zone (Fig.15)	**Chemical composition, wt.%**						
	Zr	**U**	**Fe**	**Cr**	**Ni**	**O**	**Ta**
Droplet of melt No.1 (in total)	76.0	9.0	0.5	-	-	14.5	-
Droplet of melt No.2 (in total)	77.0	9.0	0.5	-	-	12.5	-

Table 4. Results of EDX analysis of the melt (Z = 652 mm)

Description of zone (Fig.15)	Chemical composition, wt.%						
	Zr	U	Fe	Cr	Ni	O	Ta
Droplet of melt A (in total)	83.5	0.1	8.9	2.3	1.3	3.9	-
Dark phase	73.4	-	14.1	8.5	0.5	3.5	-
Bright phase	92.2	-	2.2	0.7	0.3	4.6	-
Grey phase	76.7	0.6	13.9	0.9	3.6	4.4	-
Droplet of melt B (in total)	77.7	10.5	0.6	0.1	0.1	10.9	-
Bright phase	29.4	53.1	0.2	-	-	17.3	-
Grey phase	85.4	3.5	0.1	-	-	11.1	-
Droplet of melt C (in total)	79.9	8.6	1.0	0.2	0.3	10.0	-
Dark phase	66.3	9.1	0.5	-	-	24.2	-
Bright phase	28.2	54.9	0.6	-	0.2	16.2	-
Grey phase	86.7	3.9	0.4	-	-	9.1	-

Table 5. Results of EDX analysis of the melt (Z = 679 mm)

Description of zone (Fig.16)	Chemical composition, wt.%						
	Zr	U	Fe	Cr	Ni	O	Ta
Melt A (in total)	74.4	11.6	0.3	-	-	13.7	-
Melt B (in total)	71.1	14.0	0.6	0.1	0.3	13.9	-
Melt C (in total)	76.0	10.1	0.6	0.1	0.1	13.2	-

Table 6. Results of EDX analysis of the melt (Z = 699 mm)

Description of zone (Fig.18)	Chemical composition, wt.%						
	Zr	U	Fe	Cr	Ni	O	Ta
Melt A (in total)	77.2	9.5	5.2	1.3	1.7	5.2	-
Dark phase	89.2	2.6	0.9	0.2	0.3	6.8	-
Bright phase	63.9	15.4	10.1	1.7	4.0	4.8	-
Melt B (in total)	71.8	13.8	0.6	0.1	-	13.7	-
Dark phase	84.1	5.8	0.1	-	-	10.1	-
Bright phase	33.8	47.8	0.8	0.2	0.2	17.3	-
Melt C (in total)	76.5	10.5	0.6	0.1	0.3	12.1	

Table 7. Results of EDX analysis of the melt (Z = 724 mm)

Description of zone (Fig.23)	Chemical composition, wt.%						
	Zr	U	Fe	Cr	Ni	O	Ta
Melt A (in total)	73.7	12.4	0.2	-	-	13.8	-
Melt B (in total)	70.5	15.0	0.4	0.1	0.1	13.9	-
Melt C (in total)	72.2	13.0	0.4	-	-	14.4	-

Table 8. Results of EDX analysis of the melt (Z = 745 mm)

Description of zone (Fig.26)	Chemical composition, wt.%						
	Zr	U	Fe	Cr	Ni	O	Ta
Fuel rod 2.1	43.0	31.2	0.2	-	-	25.6	-
Fuel rod 2.2	49.9	25.4	0.2	0.1	0.1	24.8	-
Fuel rod 3.1	44.5	29.5	0.1	-	-	25.9	-
Fuel rod 3.3	40.3	34.7	-	-	-	24.9	-

Table 9. Results of EDX analysis of the melt (Z = 793 mm)

Description of zone (Fig.29)	**Chemical composition, wt.%**						
	Zr	**U**	**Fe**	**Cr**	**Ni**	**O**	**Ta**
Melt A (in total)	**74.1**	**12.4**	**-**	-	-	**13.5**	-
Melt B (in total)	**58.6**	**15.2**	**-**	-	-	**25.9**	**0.3**
Melt C (in total)	**61.1**	**18.2**	**0.2**	-	**0.1**	**19.0**	**1.3**

Table 10. Results of EDX analysis of the melt (Z = 839…1066 mm)

Description of zone	**Z, mm**	**Chemical composition, wt.%**						
		Zr	**U**	**Fe**	**Cr**	**Ni**	**O**	**Ta**
Fuel rod 2.4	839	**45.9**	**26.8**	**0.1**	-	**0.1**	**27.1**	-
Fuel rod 3.4	839	**45.4**	**28.8**	-	-	-	**25.8**	-
Fuel rod 2.4	886	**36.0**	**38.1**	**0.2**	-	**0.1**	**25.6**	-
Fuel rod 2.5	886	**40.3**	**33.7**	-	-	-	**26.0**	-
Fuel rod 2.3	930	**36.9**	**37.3**	-	-	-	**25.8**	-
Fuel rod 2.5	930	**35.0**	**39.0**	-	-	-	**26.0**	-
Fuel rod 2.5	976	**34.3**	**40.3**	-	-	-	**25.4**	-
Fuel rod 3.9	976	**33.9**	**40.5**	-	-	-	**25.7**	-
Fuel rod 2.1	1021	**55.7**	**16.4**	-	-	**1.2**	**26.4**	**0.4**
Fuel rod 2.4	1021	**50.6**	**22.3**	-	-	-	**27.1**	-
Fuel rod 2.4	1066	**66.0**	**14.8**	**0.2**	-	-	**19.1**	-
Fuel rod 3.2	1066	**67.9**	**15.5**	-	-	-	**15.5**	-

PICTURES

Fig. 1. External appearance of the thermal insulation housing inner surface at the level of 700-1300 mm.

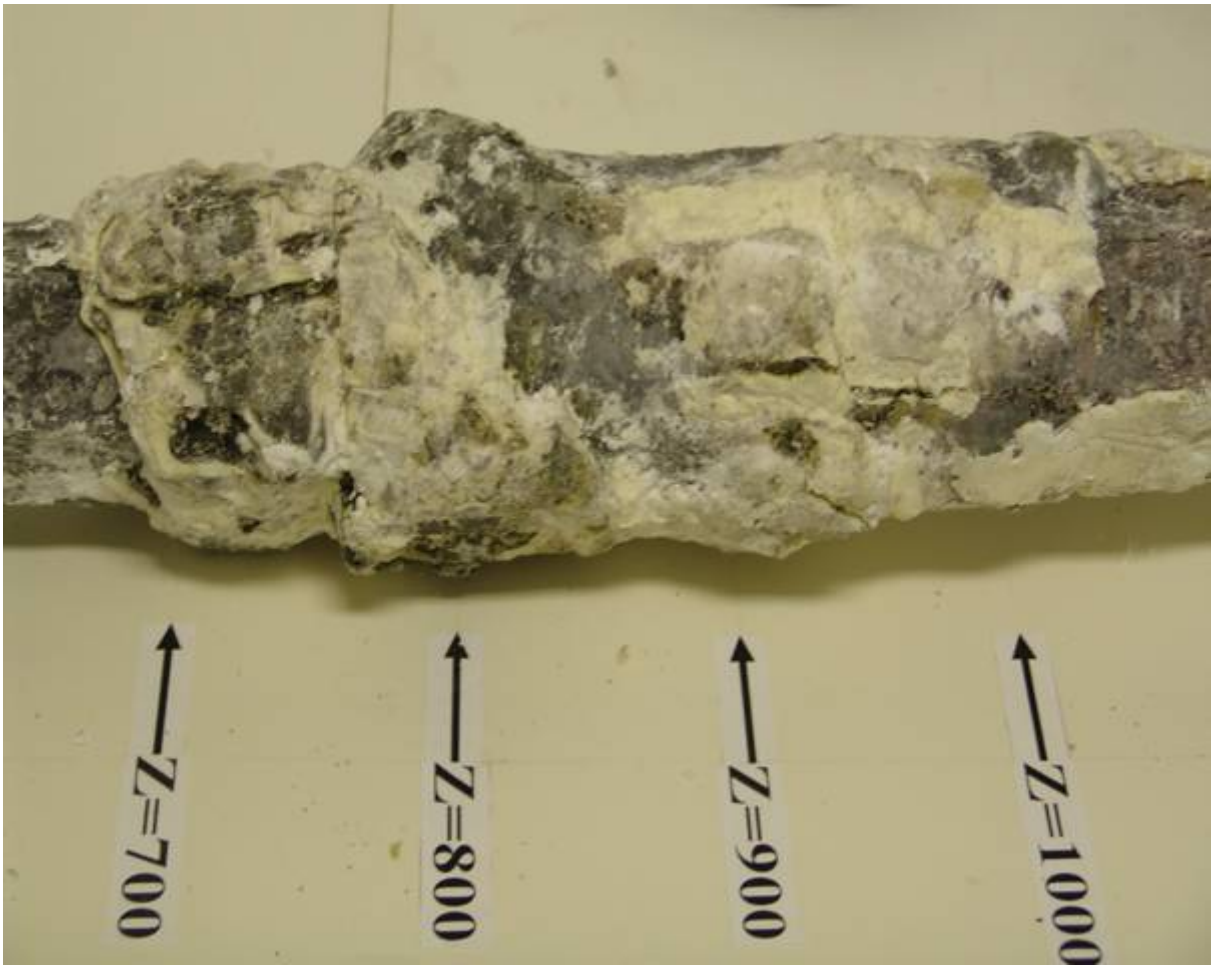

Fig. 2. External appearance of the shroud after the tests (level 700 – 1000 mm, 90^{o} – 120^{o}).

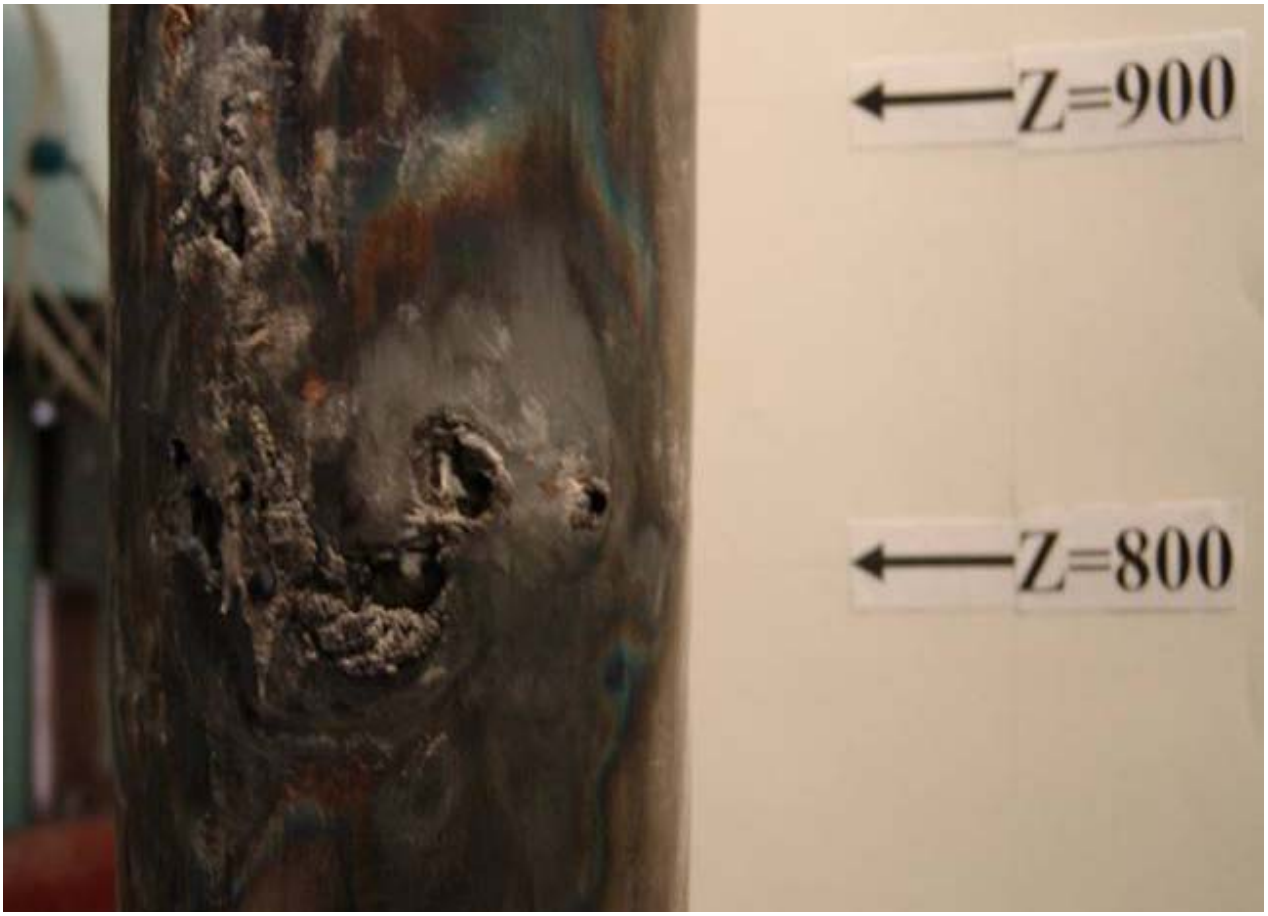

Fig. 3. External appearance of the thermoinsulation at the level of 700 – 900 mm after the experiment.

Fig. 4. External appearance of the thermoinsulation with traces of melting at the level of 700 – 1000 mm.

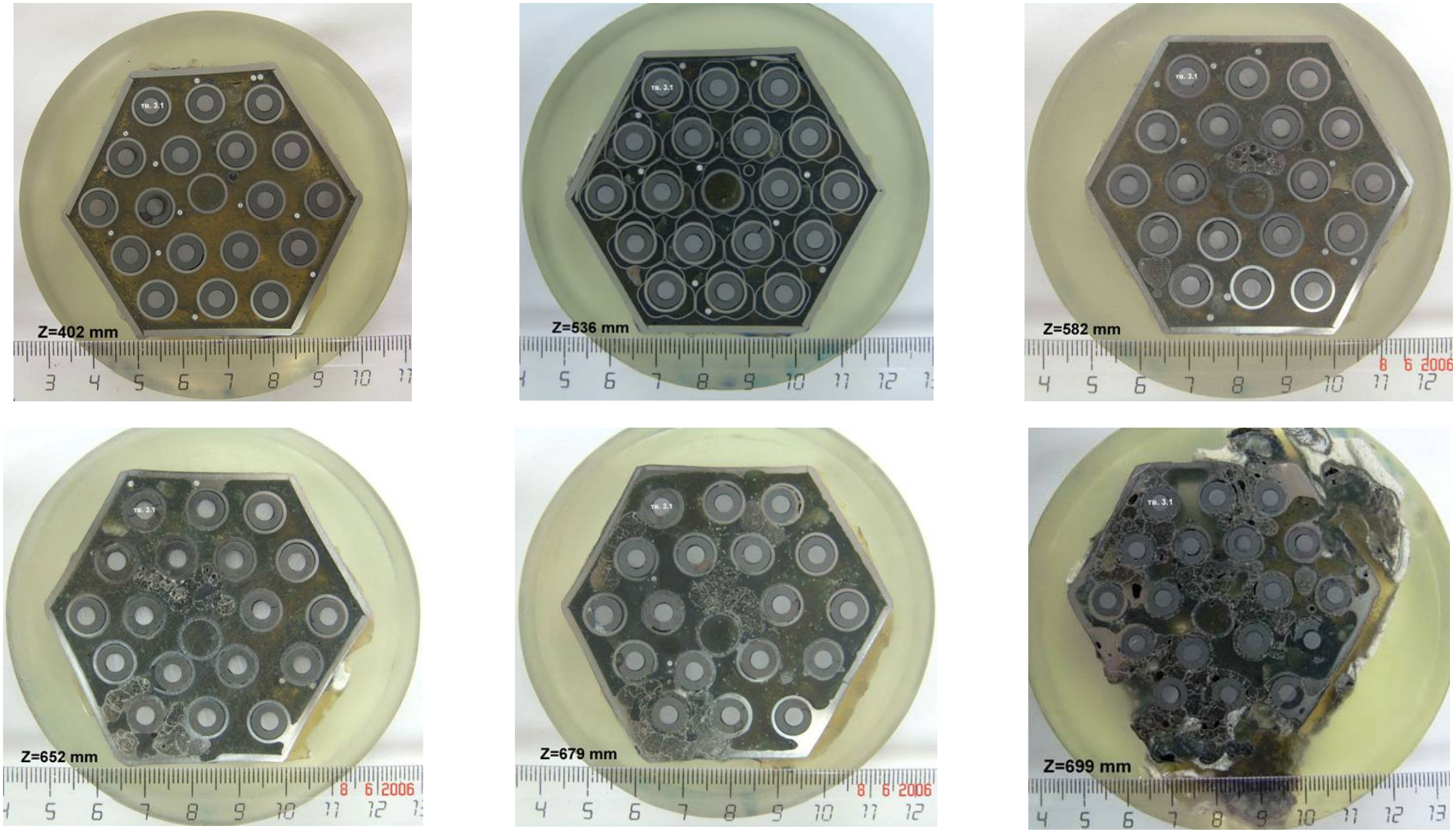

Fig. 5. Photos of the assembly elevation cross-sections ~ 400 – 700 mm.

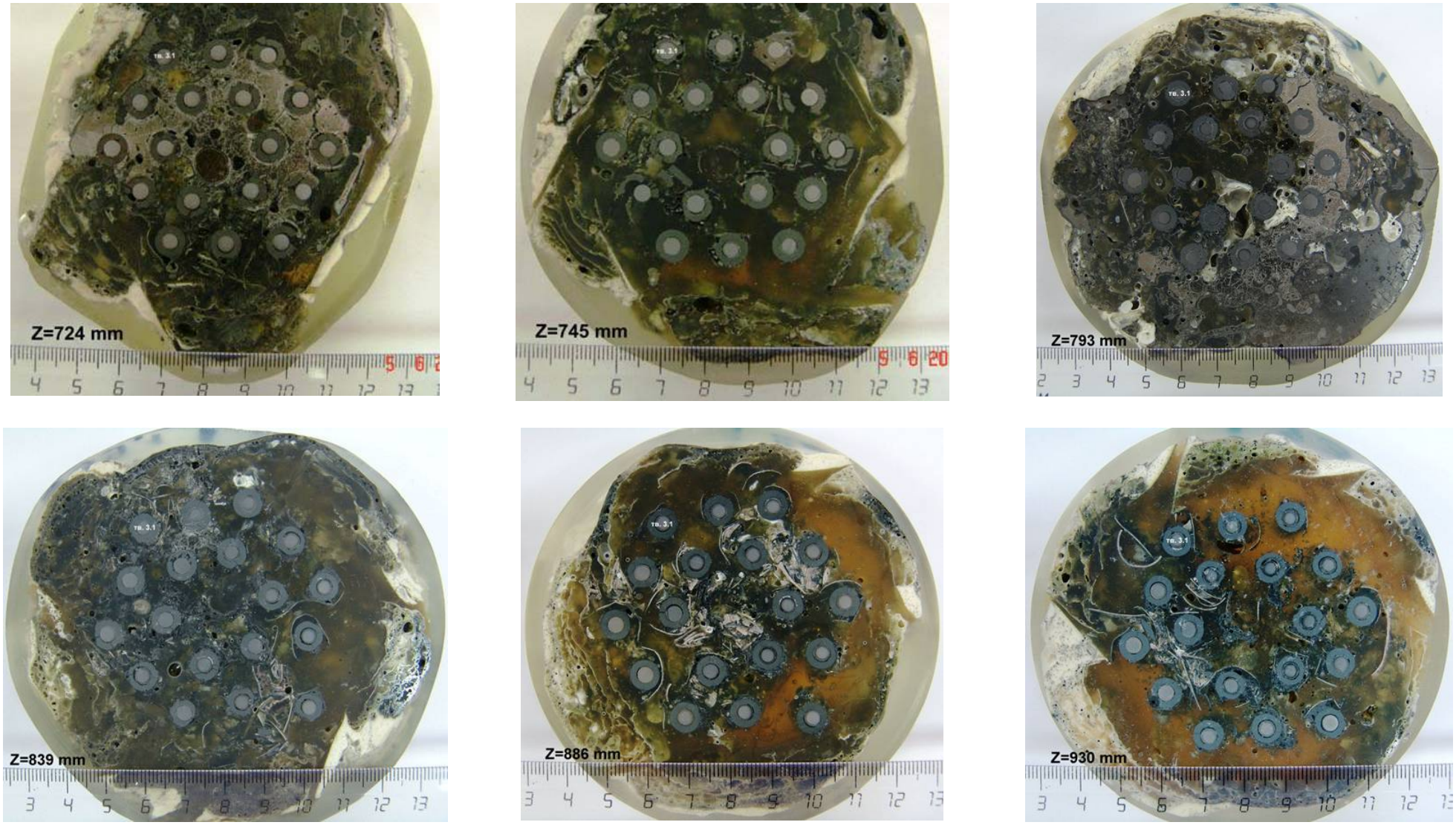

Fig. 6. Photos of the assembly elevation cross-sections ~ 700 – 950 mm.

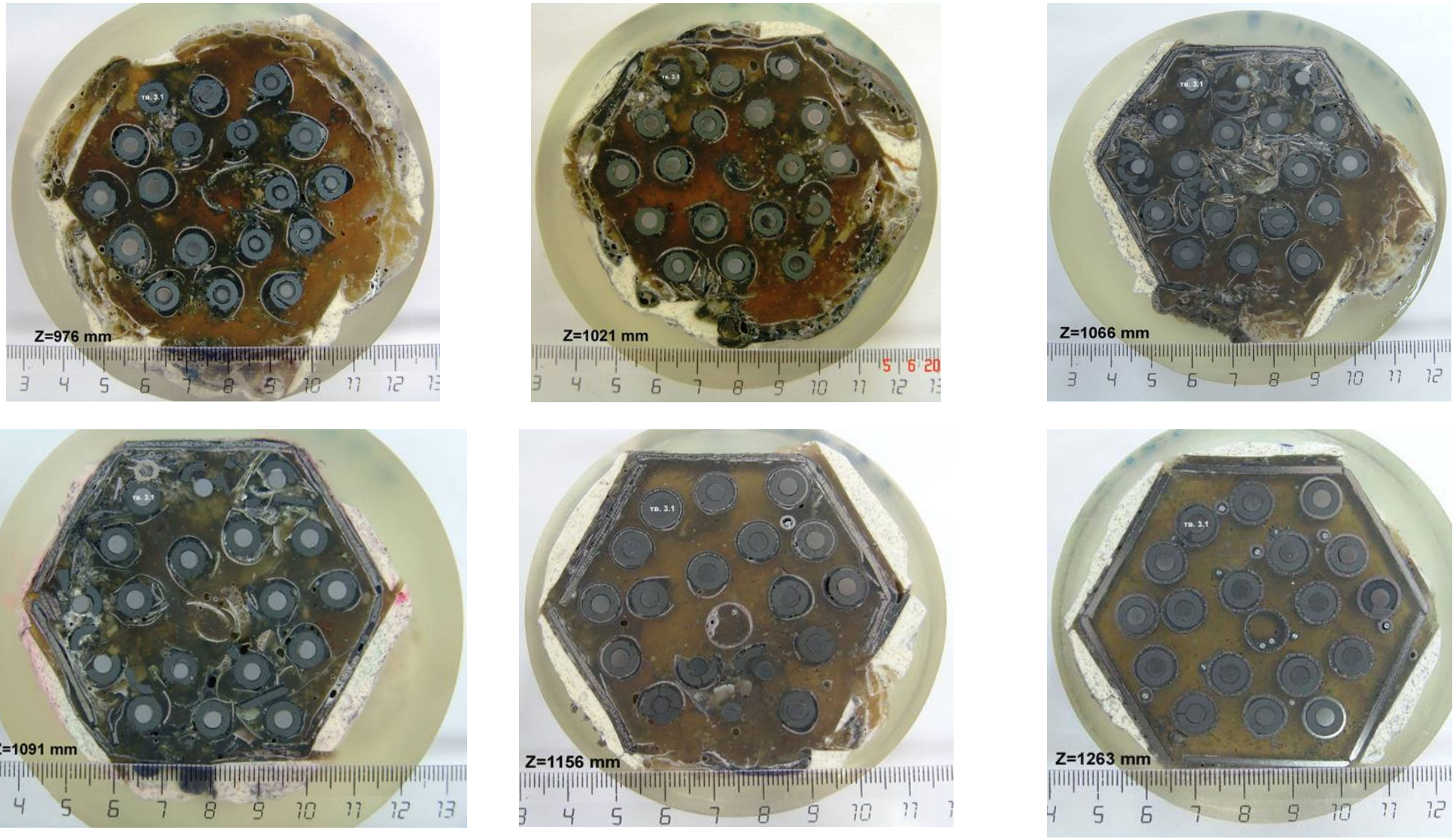

Fig. 7. Photos of the assembly elevation cross-sections ~ 950 – 1300 mm.

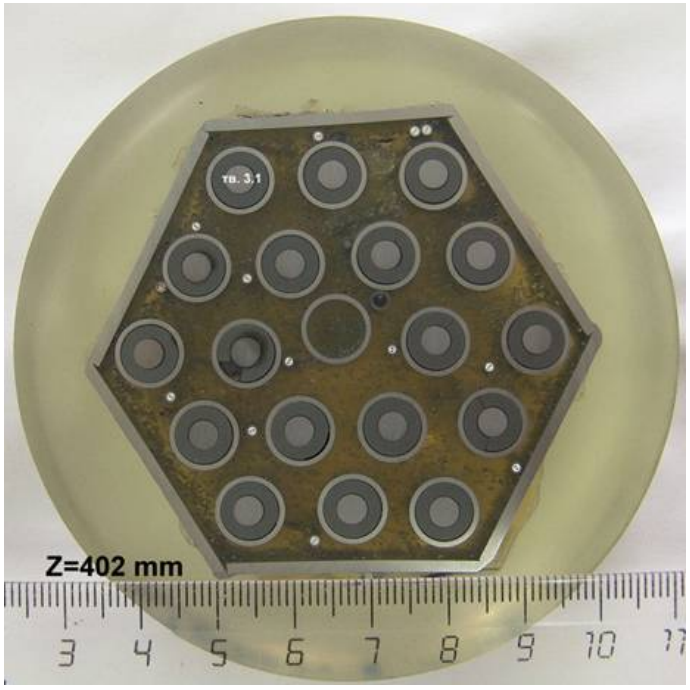

Fig. 8. Cross-section of the assembly at the level of 402 mm (top view).

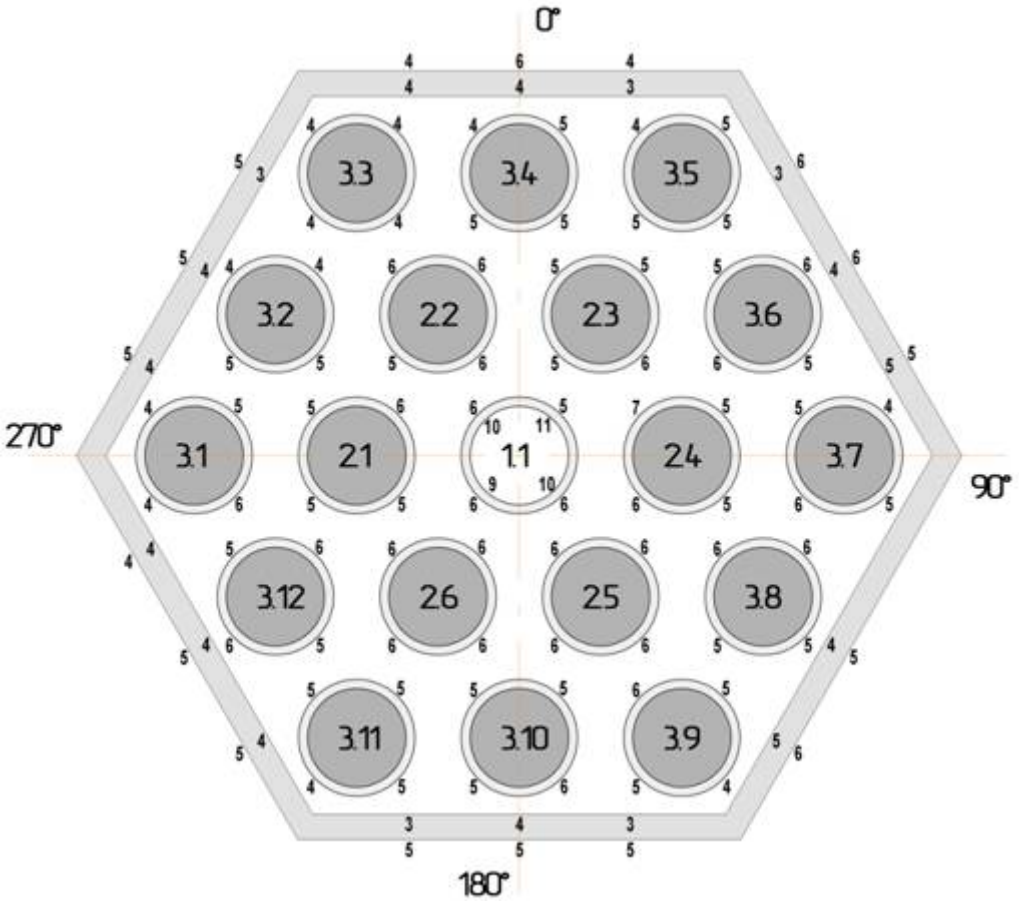

Fig. 9. Thickness of oxide layer on the surface of housing and shrouds at the level of 402 mm (top view).

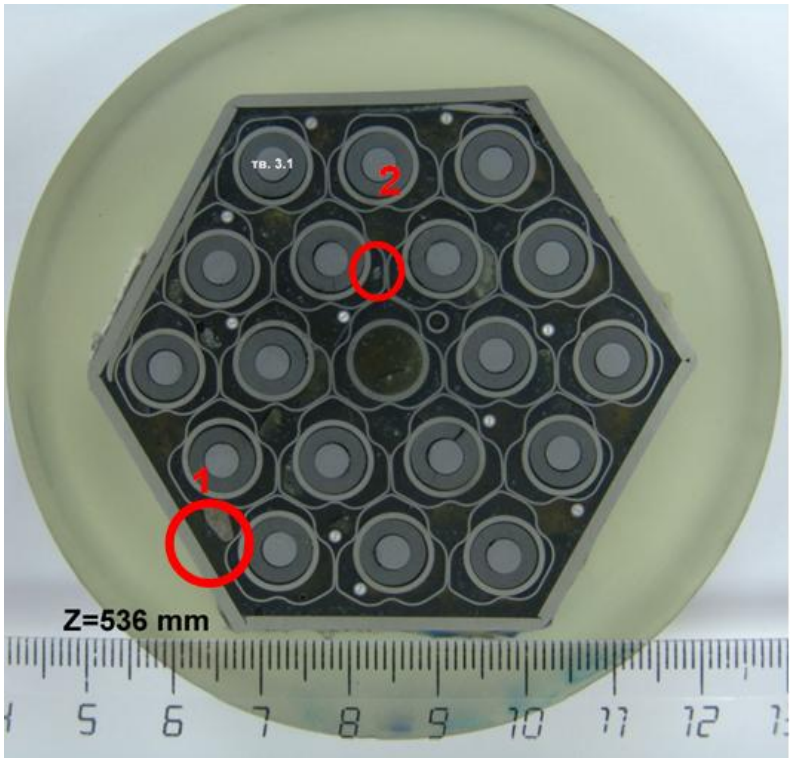

Fig. 10. Cross-section of the assembly at the level of 536 mm (top view).

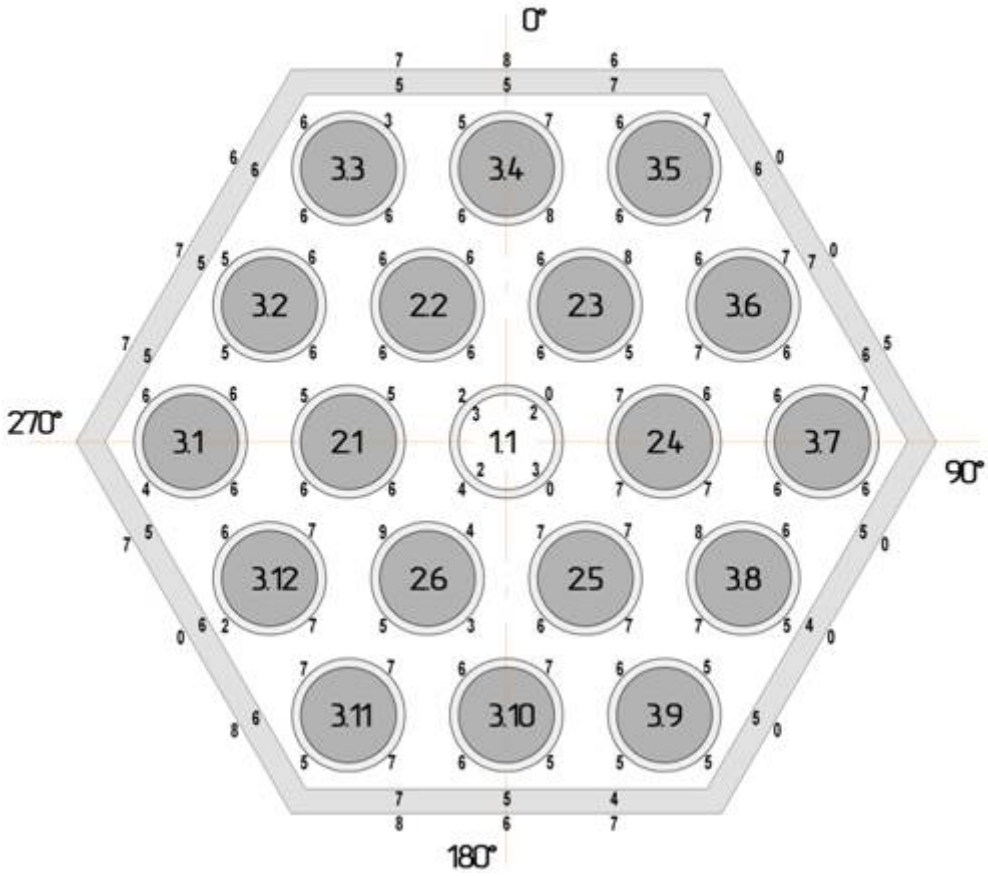

Fig.11. Thickness of oxide layer on the surface of housing and shrouds at the level of 536 mm.

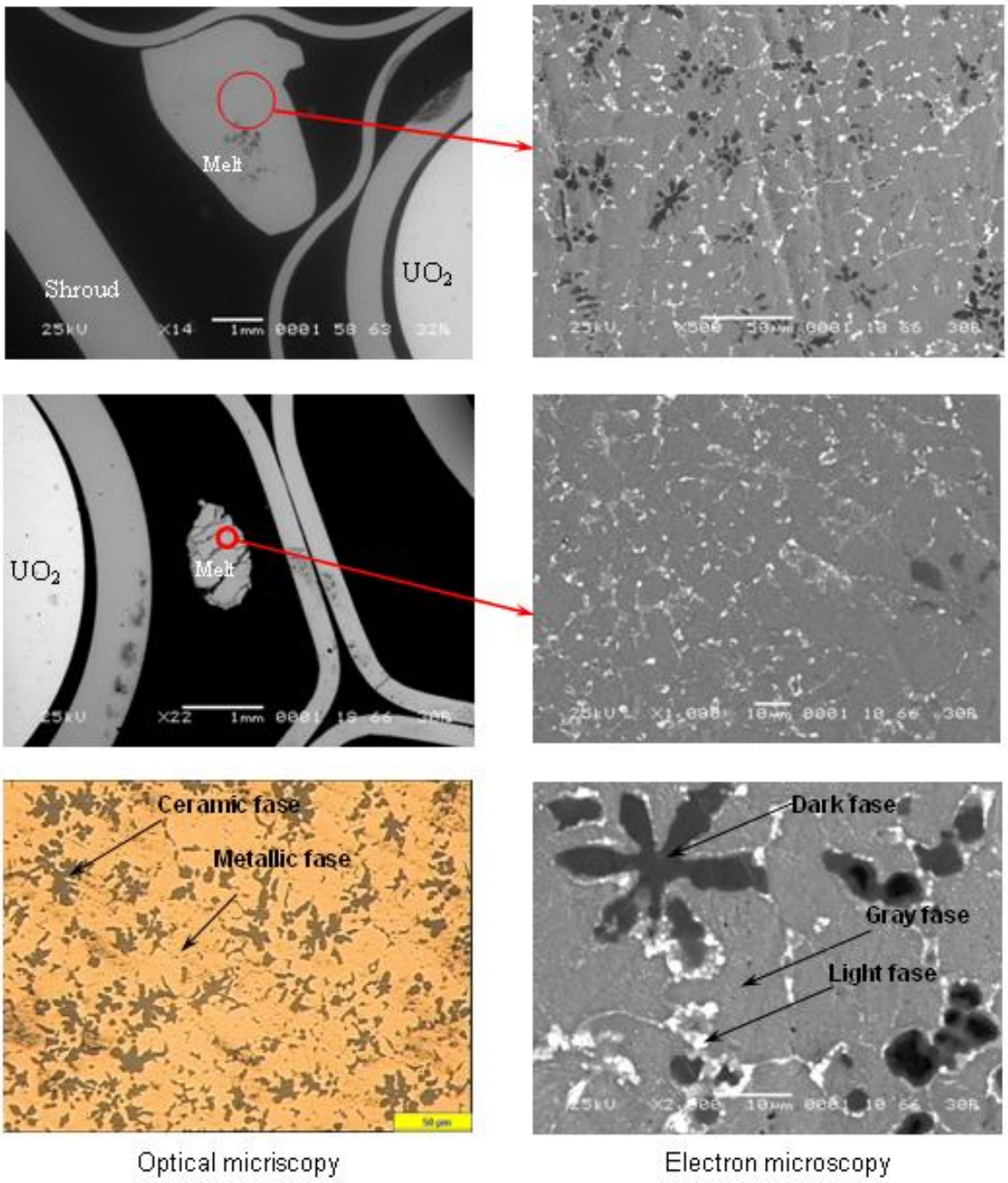

Ceramic faze content ~ 24 vol %.

Chemical composition, weight %.
Zr - 77.6
U - 9.0
Fe - 0.3
Cr - 0
Ni - 0
O - 13.0

Fig. 12. Microstructure of cross-section 536 mm
of the model assembly PARAMETER–SF1. Melt droplets (Zr, U, O).

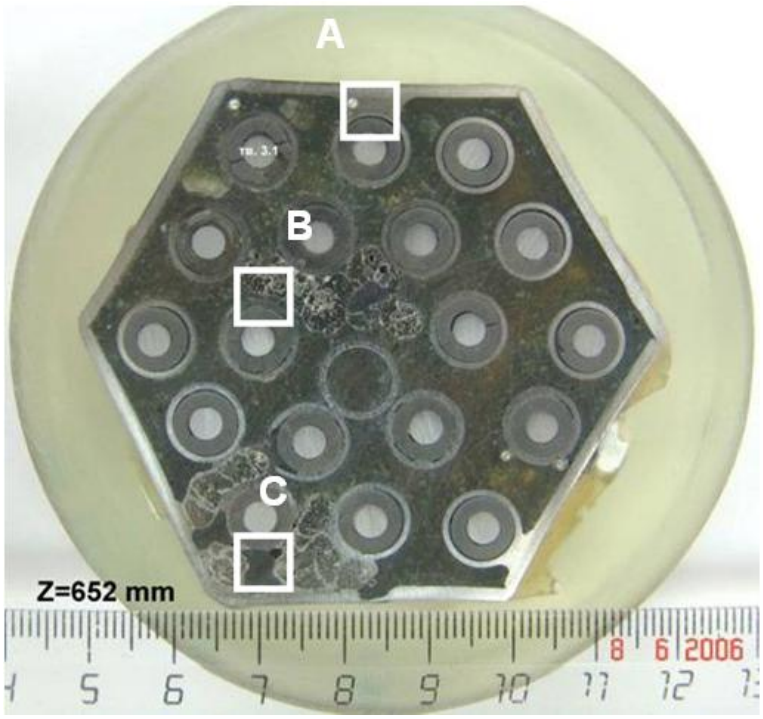

Fig. 13. Cross-section of the assembly at the level of 652 mm (top view).

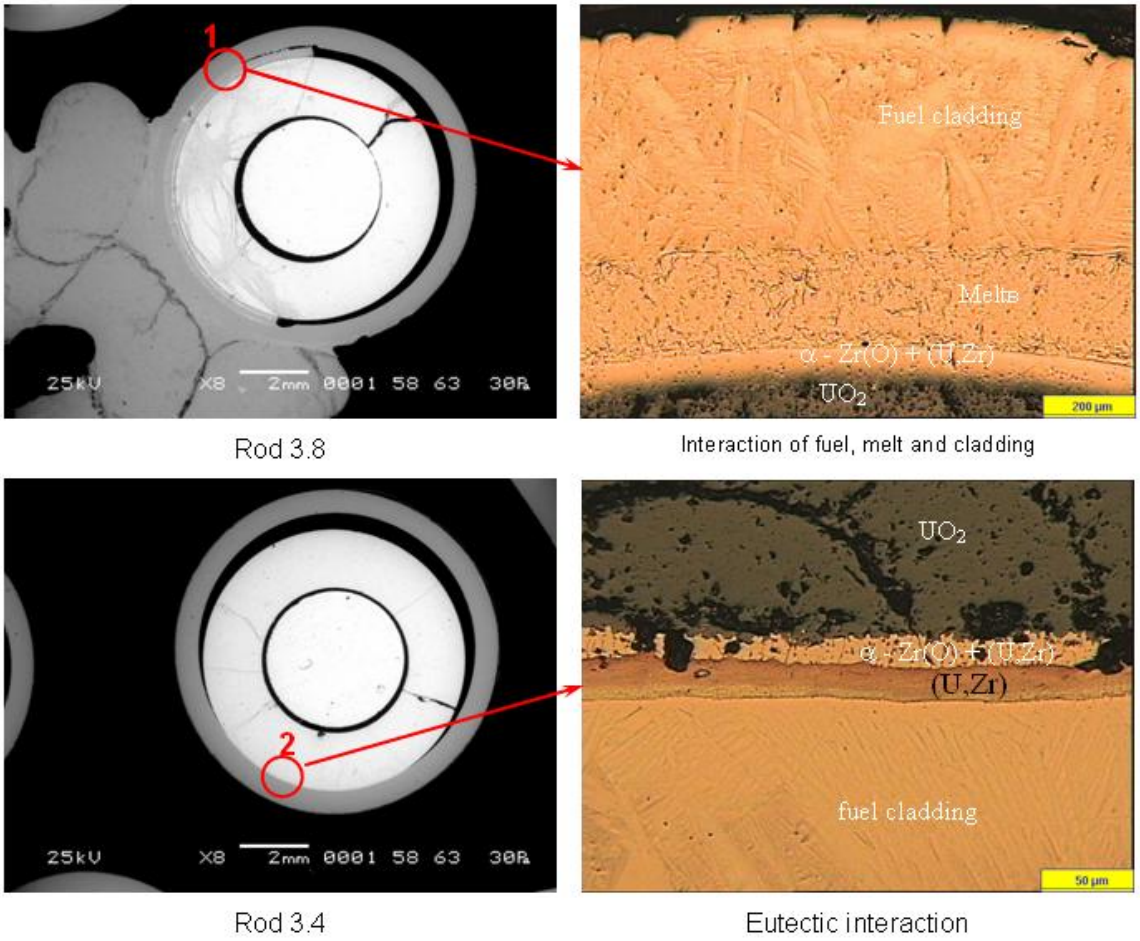

Fig. 14. Microstructure of cross-section 652 mm of the model assembly PARAMETER–SF1. Outer and inner melt running down.

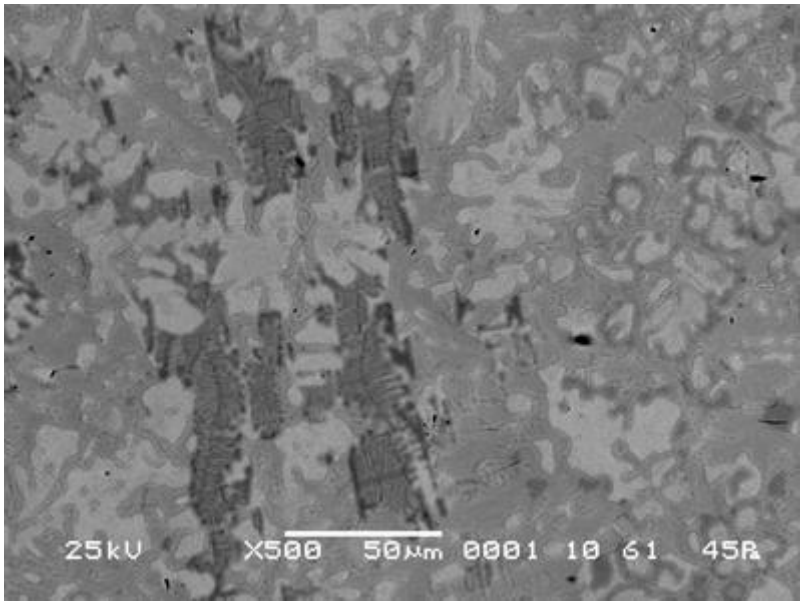

Zone A

Melt formed as result of eutectic interaction Zr – SS

Chemical composition, weight %.

Zr - **83.5**
U - **0.1**
Fe - **8.9**
Cr - **2.3**
Ni - **1.3**
O - **3.9**

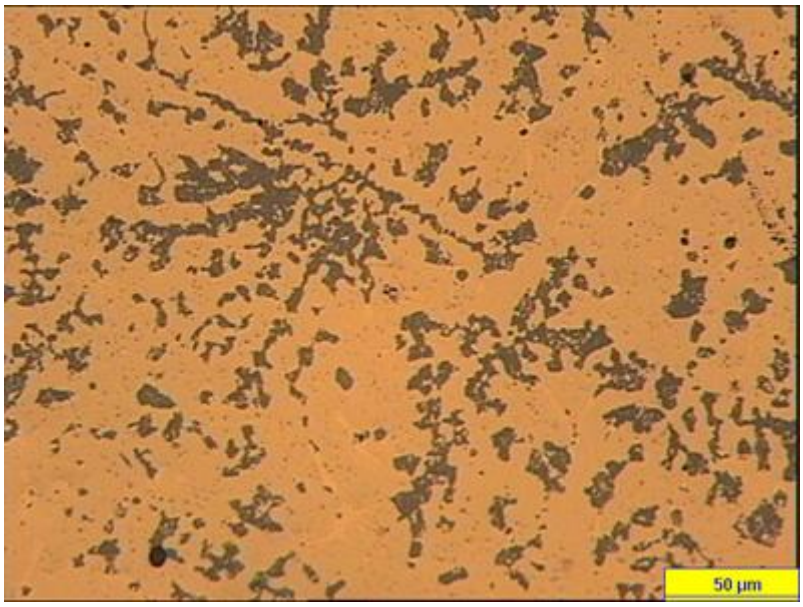

Zone Б

Melt (U,Zr,O)
Ceramic fase content
~ 22 % vol.

Chemical compositions, weight %.

Zr - **77.7**
U - **10.5**
Fe - **0.6**
Cr - **0.1**
Ni - **0.1**
O - **10.9**

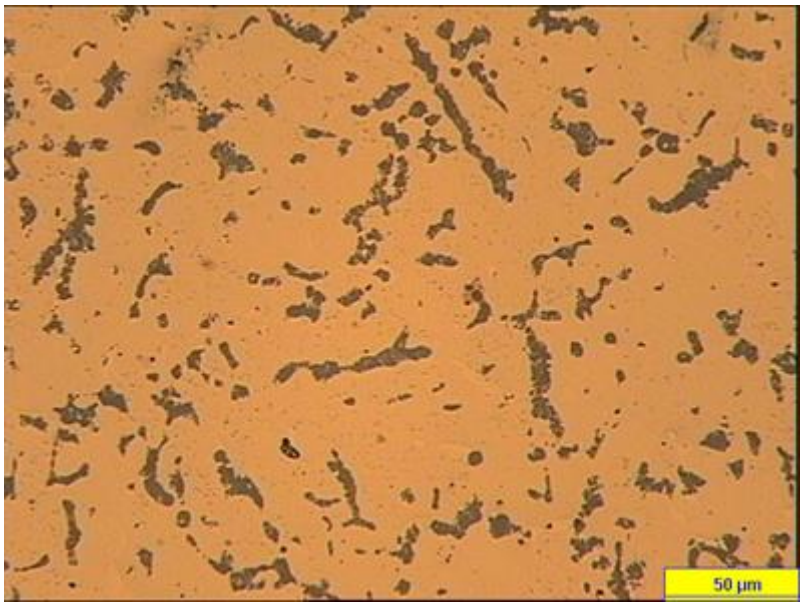

Zone C

Melt (U,Zr,O)
Ceramic fase content
~ 14 % vol.

Chemical compositions, weight %.

Zr - **79.9**
U - **8.6**
Fe - **1.0**
Cr - **0.2**
Ni - **0.3**
O - **10.0**

Fig. 15. Structures of melts from different zones in section 652 mm.

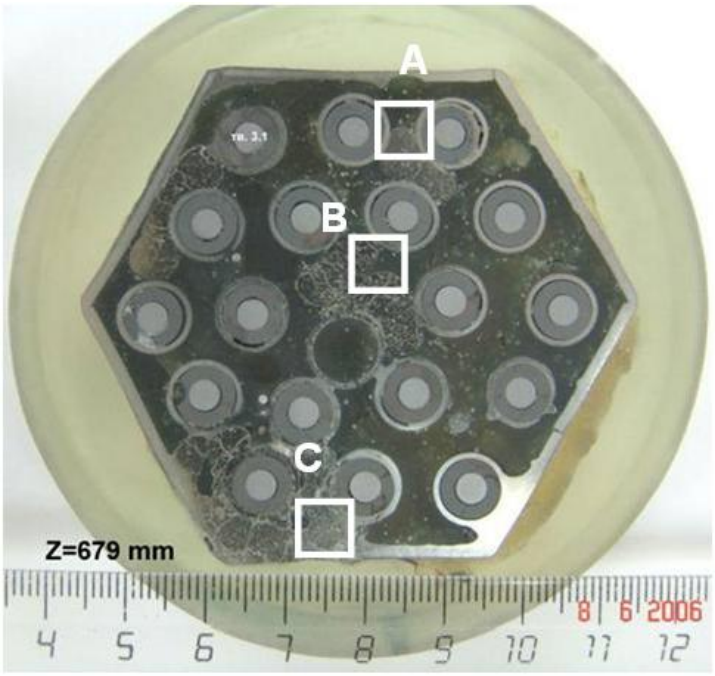

Fig. 16. Cross-section of the assembly at the level of 679 mm (top view).

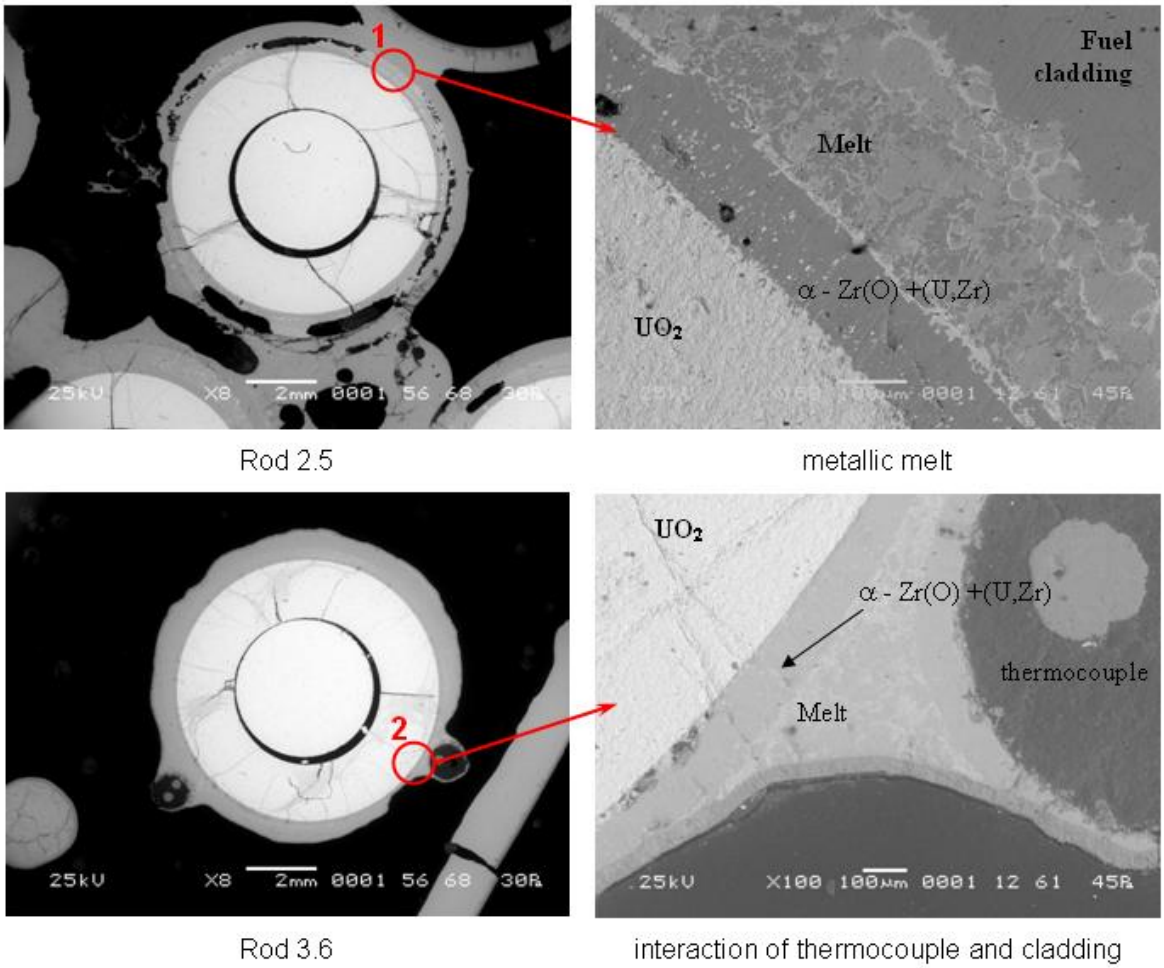

Fig. 17. Microstructure of cross-section 679 mm of the model assembly PARAMETER–SF1. Beginning of UO_2 dissolution with melted zirconium.

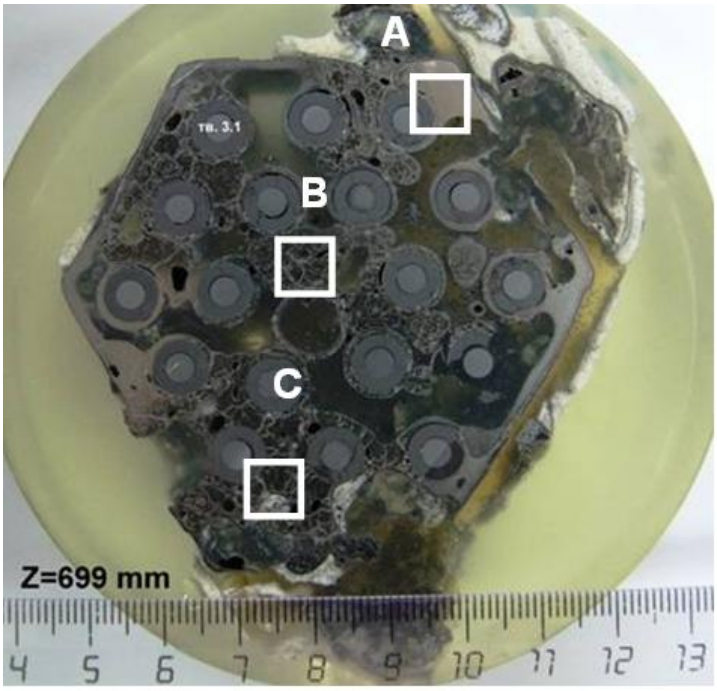

Fig. 18. Cross-section of the assembly at the level of 699 mm (top view).

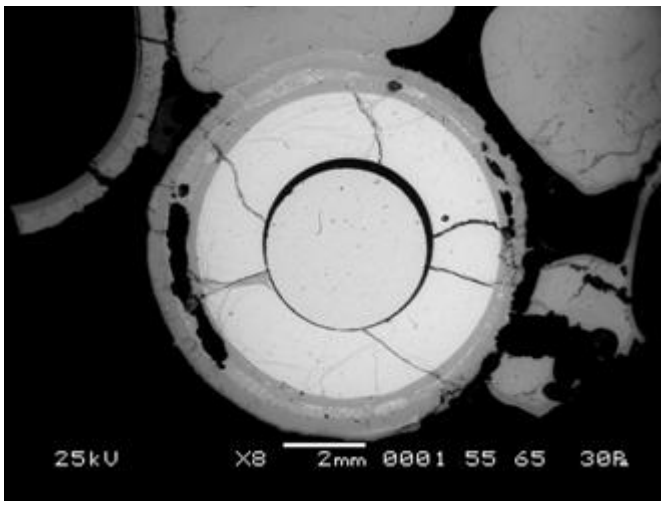

Rod 2.4

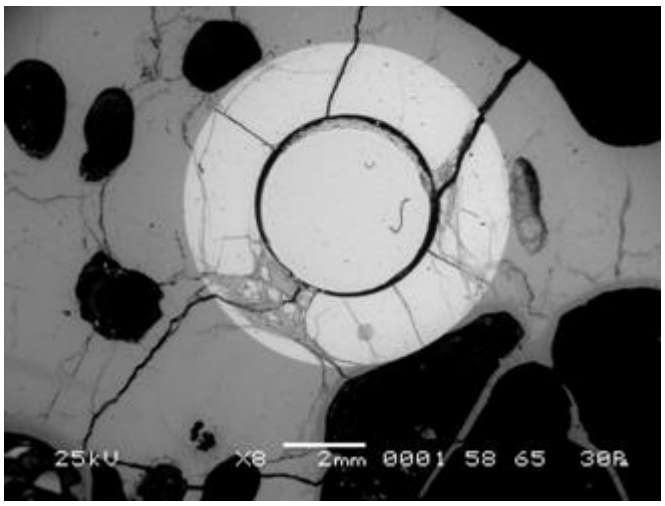

Rod 3.8

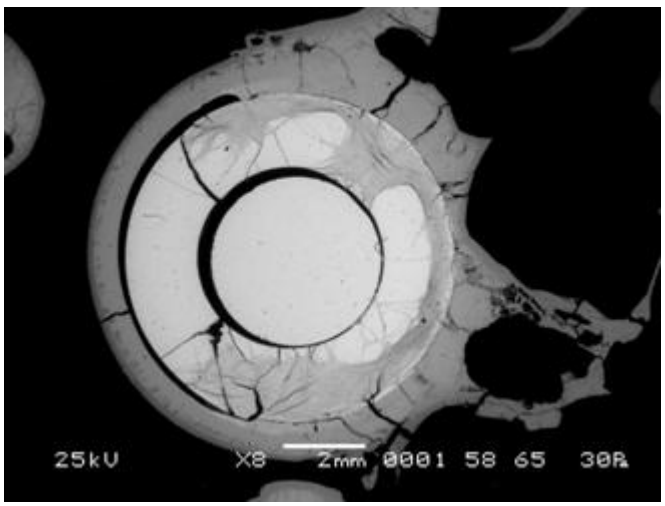

Rod 3.4

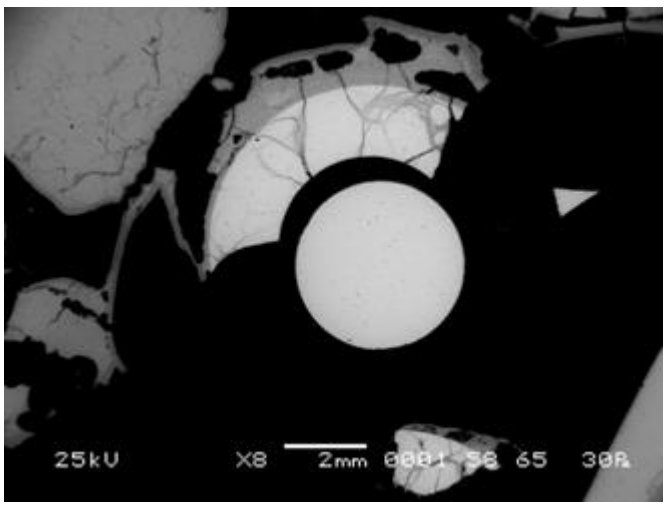

Rod 3.6

Fig. 19. Microstructure of cross-section 699 mm of the model assembly

PARAMETER–SF1. Beginning of UO_2 dissolution with melted zirconium.

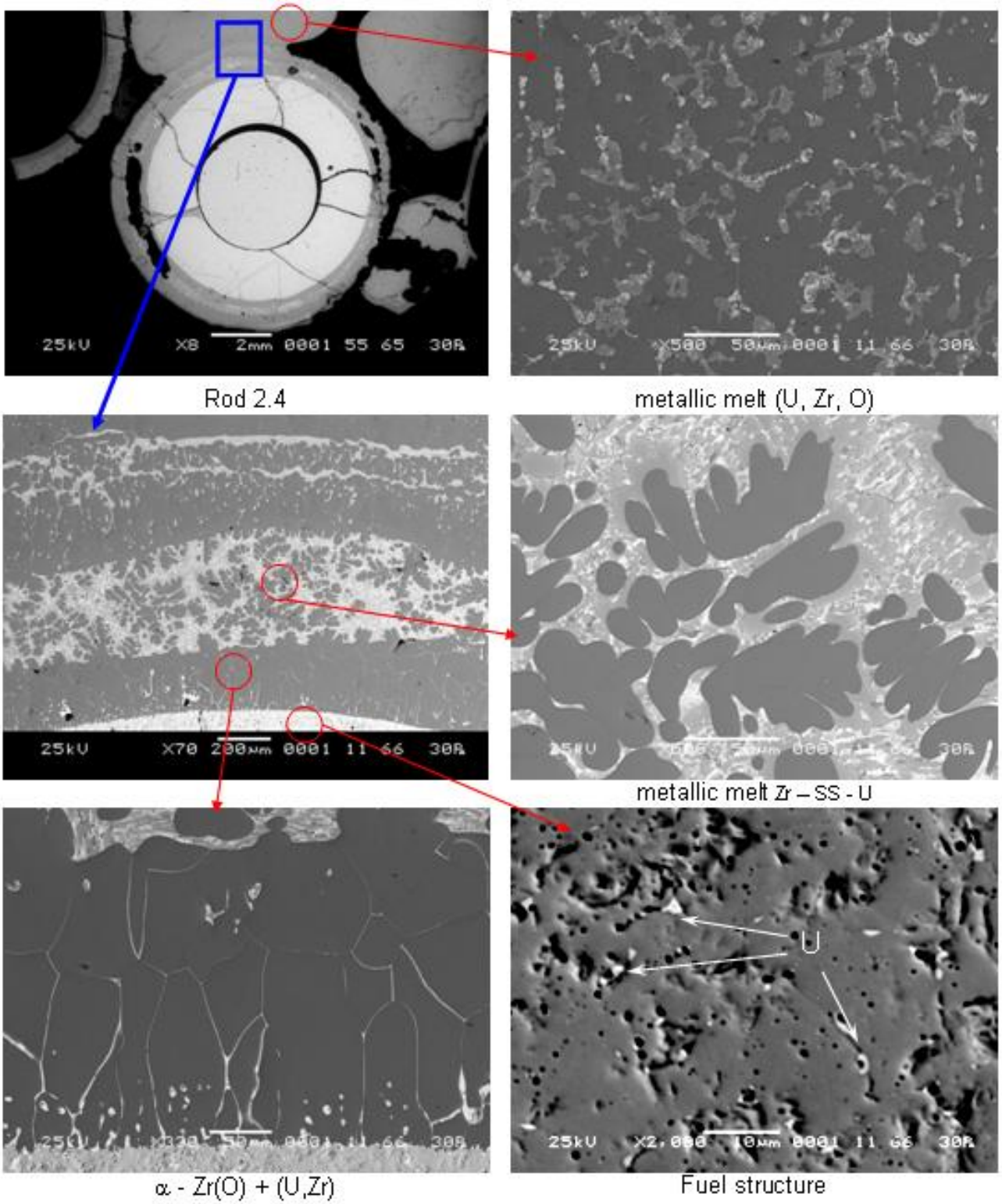

Fig. 20. Microstructure of cross-section 699 mm of the model assembly PARAMETER–SF1. Dissolution of UO_2 and ZrO_2 on the cladding surface with melted zirconium.

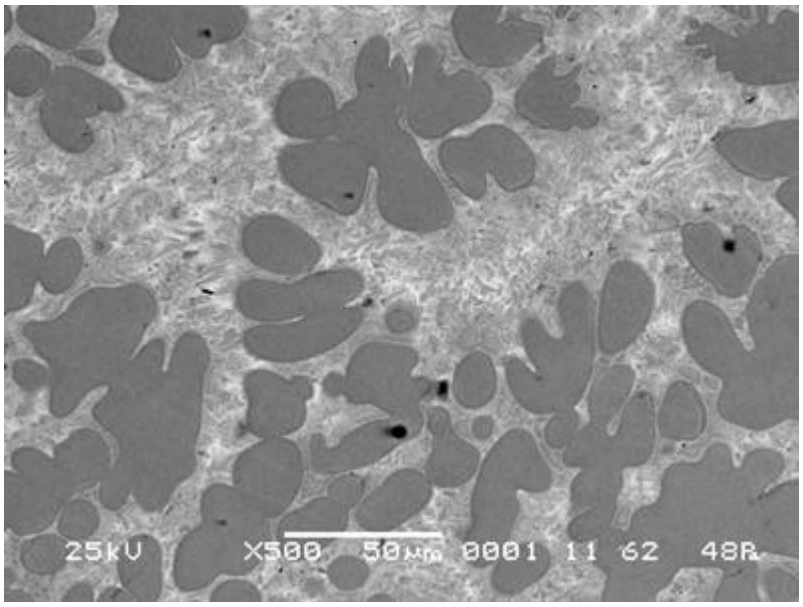

Zone A

Melt (U,Zr,O) + SS

Chemical composition, weight %.

Zr - **77.2**
U - **9.5**
Fe - **5.2**
Cr -**1.3**
Ni - **1.7**
O - **5.2**

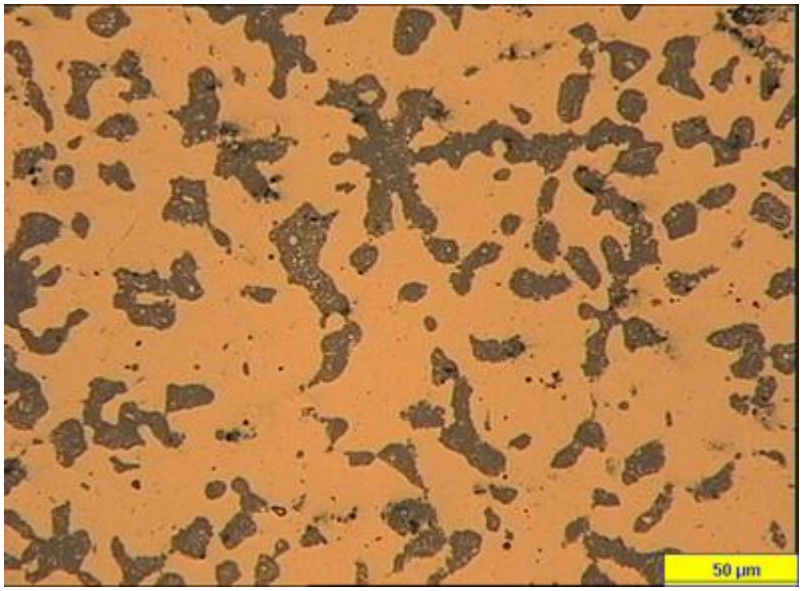

Zone Б

Melt (U,Zr,O)
Ceramic fase content
~ 22 % vol.

Chemical composition, weight %.

Zr - **71.8**
U - **13.8**
Fe - **0.6**
Cr -**0.1**
Ni - **0**
O - **13.7**

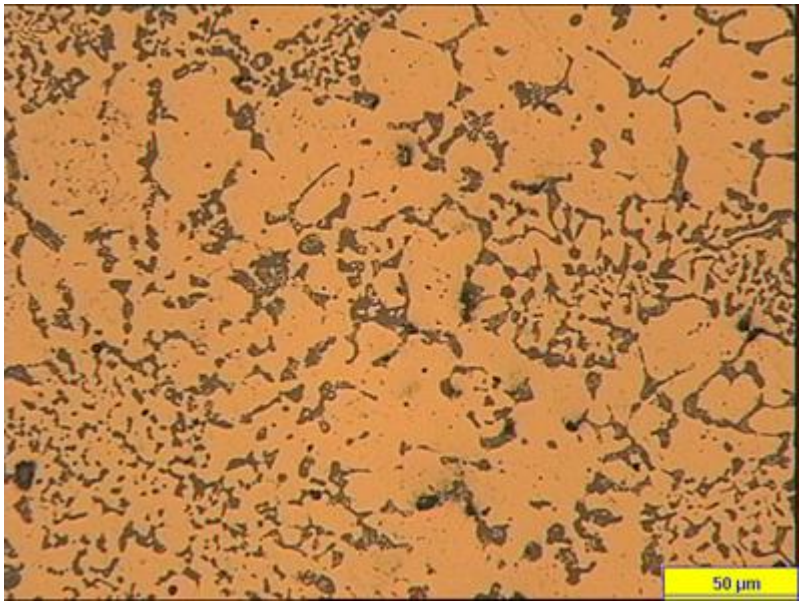

Zone C

Melt (U,Zr,O)
Ceramic fase content
~ 22 % vol.

Chemical composition, weight %.

Zr - **76.5**
U - **10.5**
Fe - **0.6**
Cr - **0.1**
Ni - **0.3**
O - **12.1**

Fig.21. Structures of melts from different zones in section 699 mm.

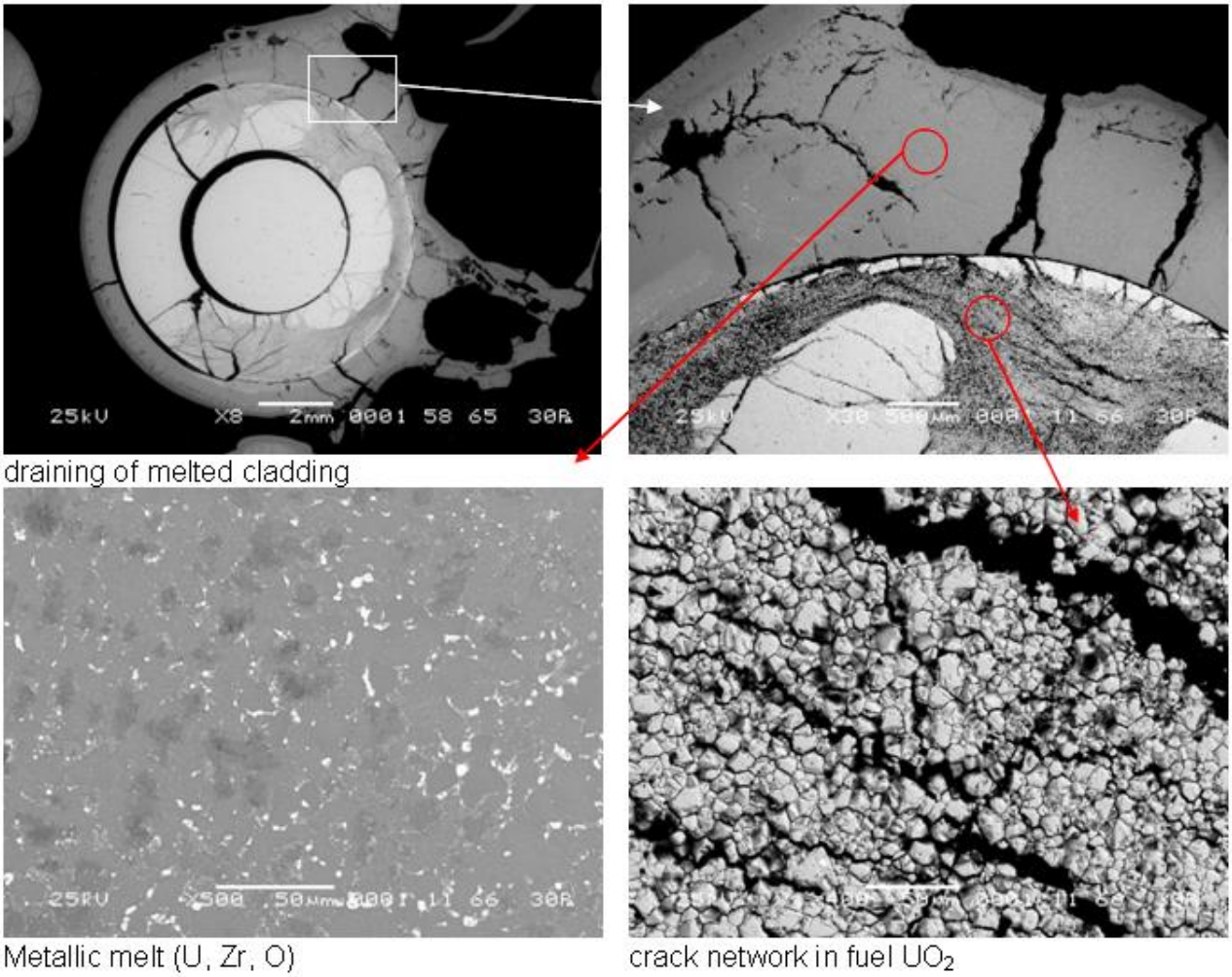

Fig. 22. Microstructure of cross-section 699 mm of the model assembly PARAMETER–SF1. Failure of fuel rod simulator 3.4.

Fig. 23. Cross-section of the assembly at the level of 724 mm (top view).

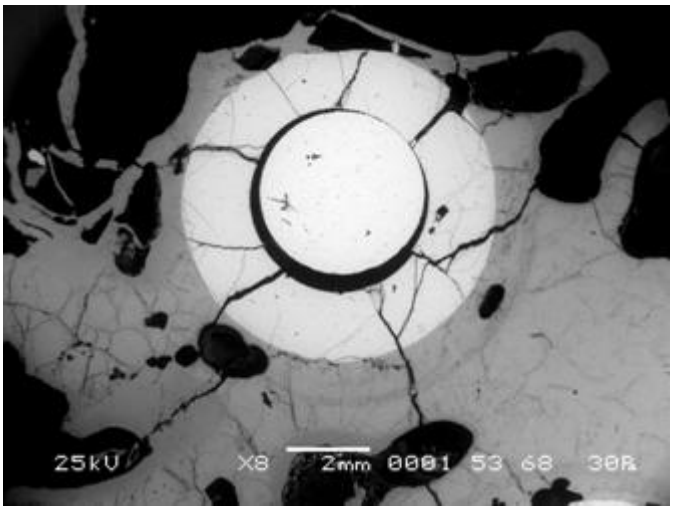

Rod 3.2

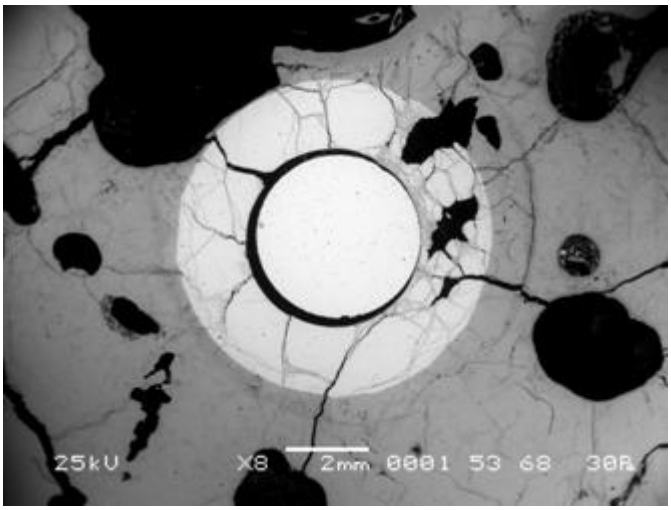

Rod 2.1

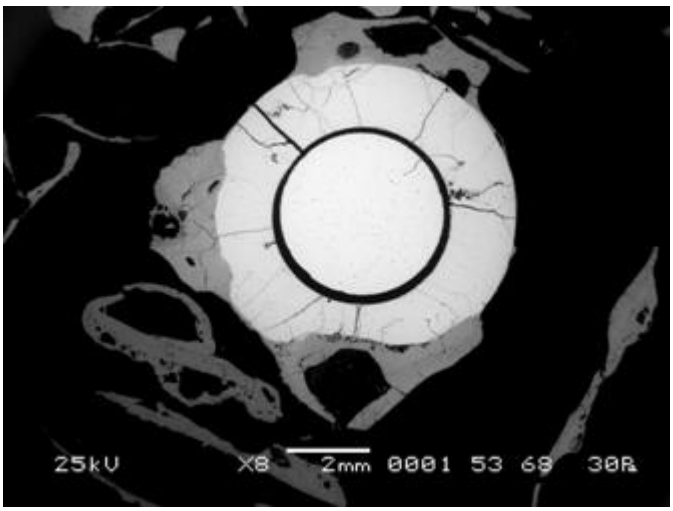

Rod 3.8

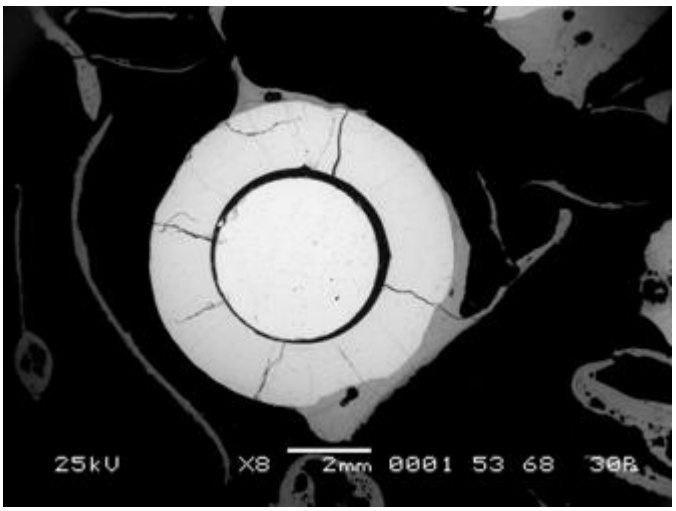

Rod 3.9

Fig. 24. Microstructure of cross-section 724 mm of the model assembly PARAMETER–SF1.

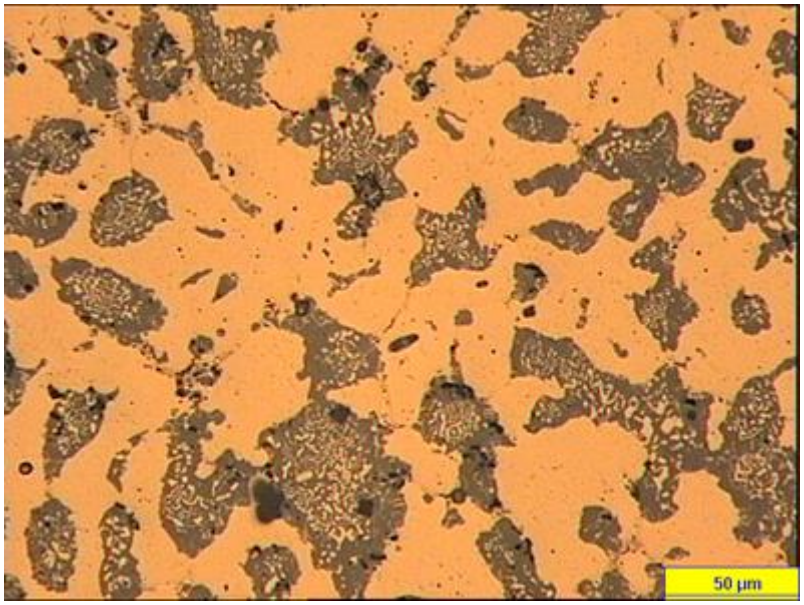

Zone A

Melt (U,Zr,O)
Ceramic faze content
~ 27% vol.

Chemical composition,
weight %.

Zr - **70.5**
U - **15.0**
Fe - **0.4**
Cr - **0.1**
Ni - **0.1**
O - **13.9**

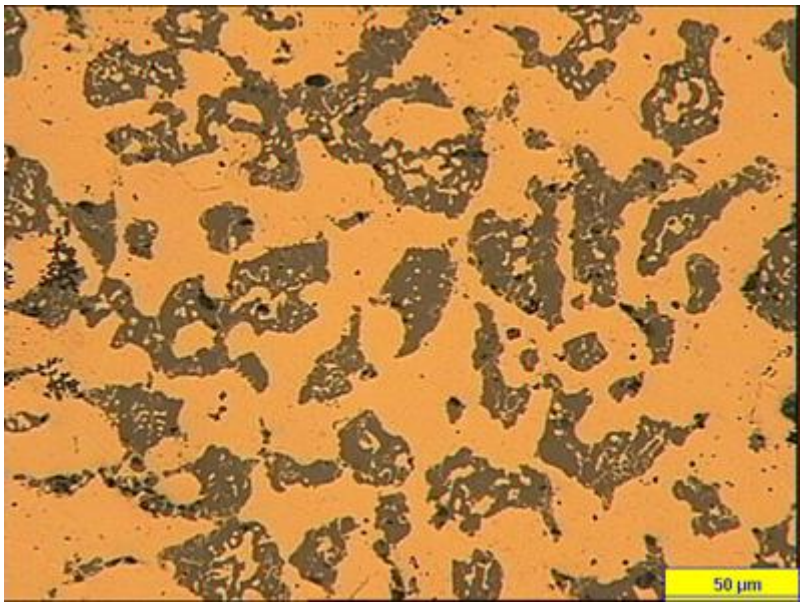

Zone B

Melt (U,Zr,O)
Ceramic faze content
~ 30 % vol.

Chemical composition,
weight %.

Zr - **72.2**
U - **13.0**
Fe - **0.4**
Cr - **0**
Ni - **0**
O - **14.4**

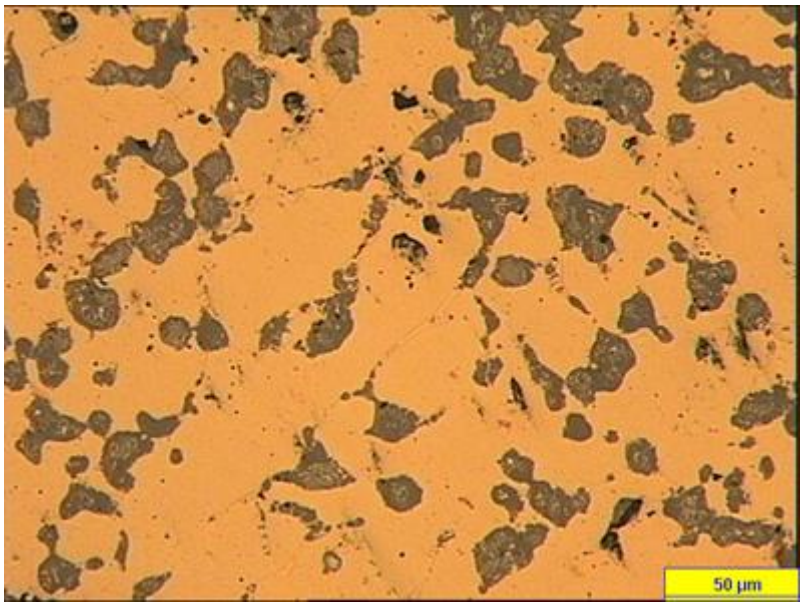

Zone C

Melt (U,Zr,O)
Ceramic faze content
~ 25 % vol.

Chemical composition,
weight %.

Zr - **73.7**
U - **12.4**
Fe - **0.2**
Cr - **0**
Ni - **0**
O - **13.8**

Fig. 25. Structures of melts from different zones of section 724 mm.

Fig. 26. Cross-section of the assembly at the level of 745 mm (top view).

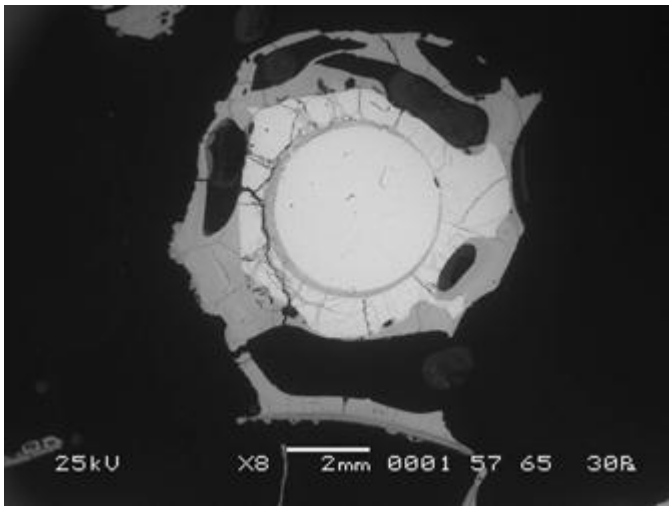

Rod 3.1

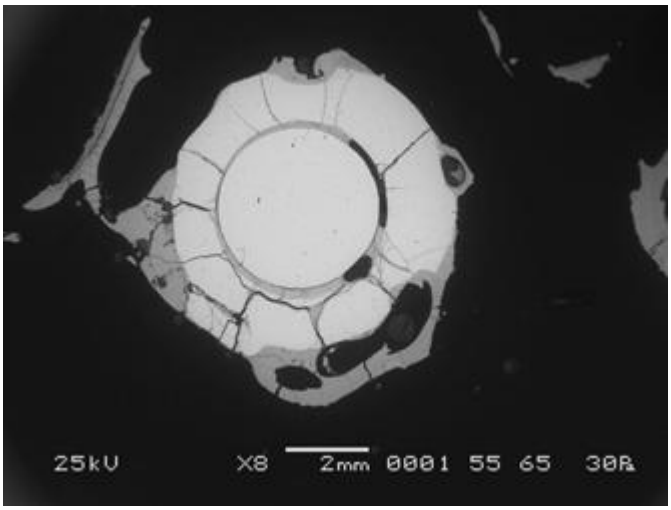

Rod 2.1

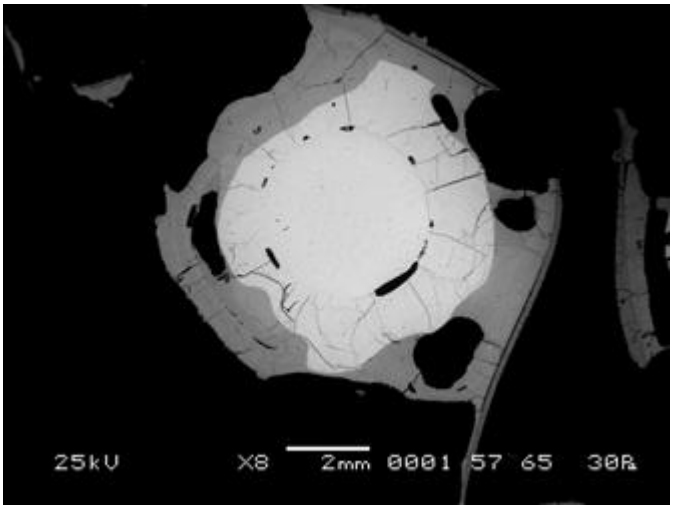

Rod 2.2

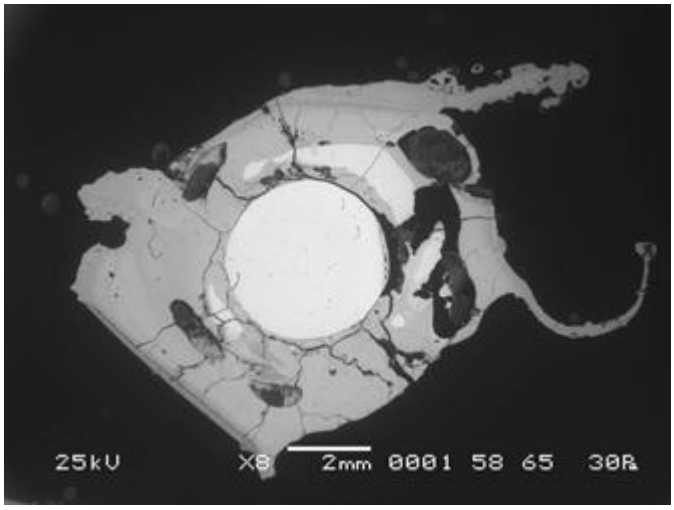

Rod 3.3

Fig. 27. Microstructure of cross-section 745 mm of the model assembly PARAMETER–SF1.

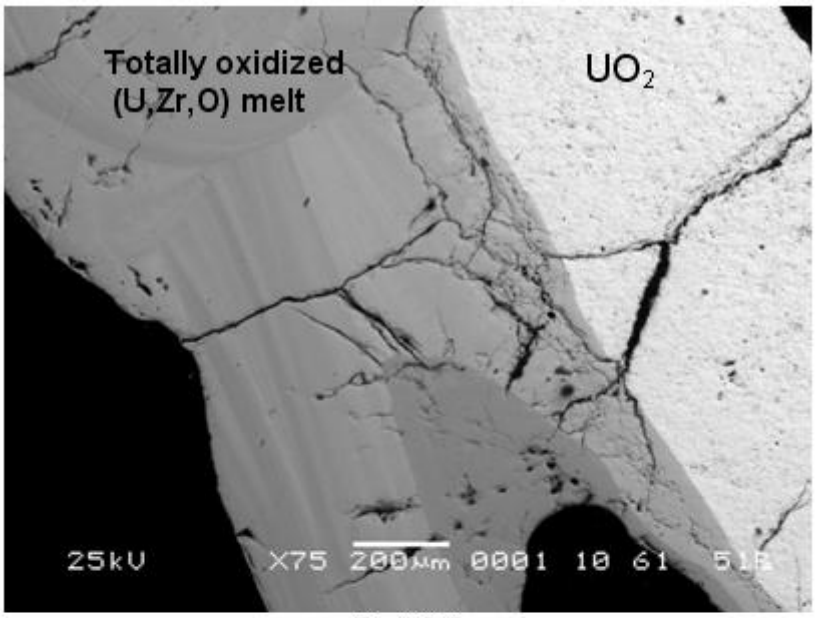

Rod 2.2

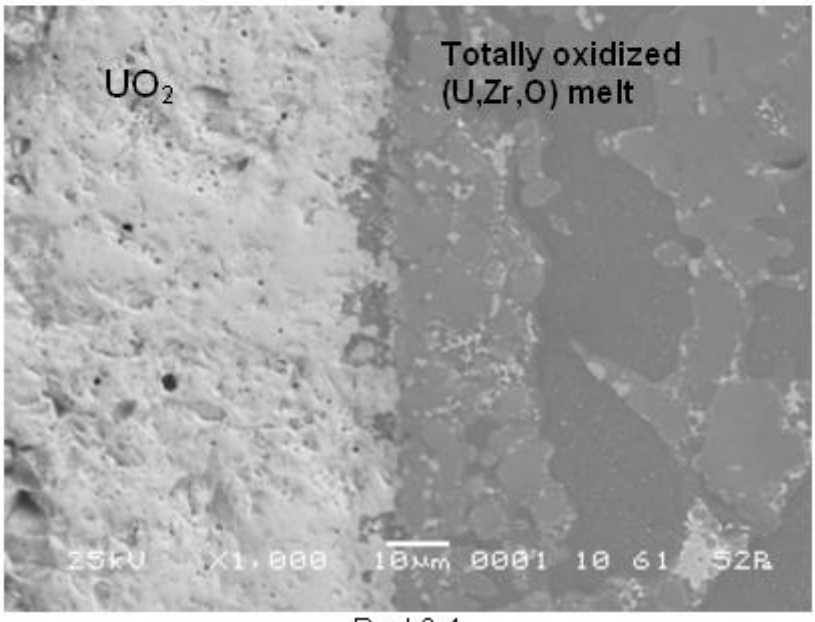

Rod 3.1

Fig. 28. Structure of UO_2 – melt (U,Zr,O) interaction zone.

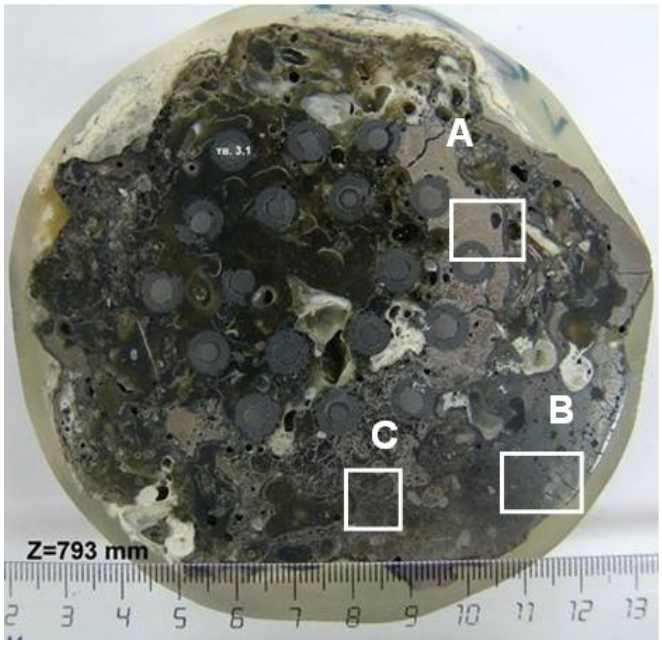

Fig. 29. Cross-section of the assembly at the level of 793 mm (top view).

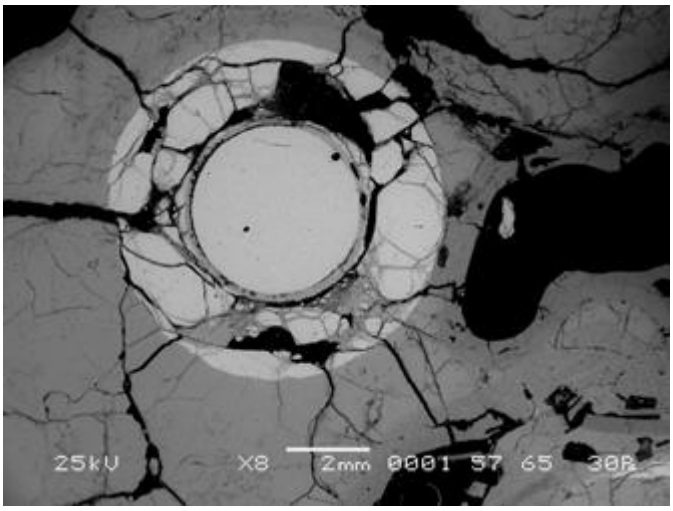

Rod 3.7

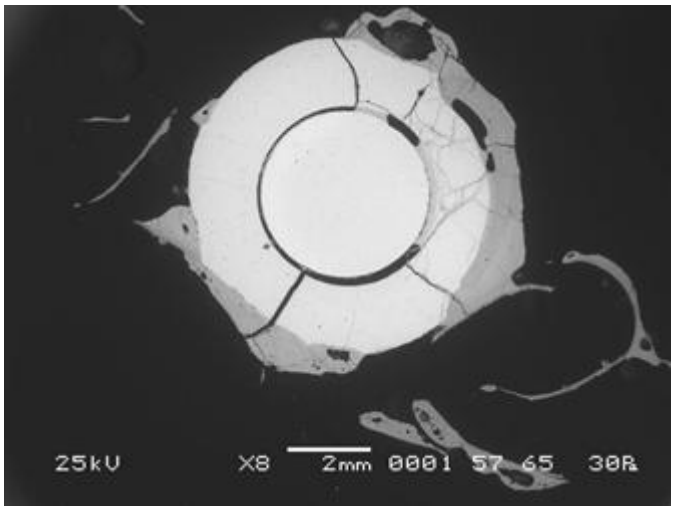

Rod 2.1

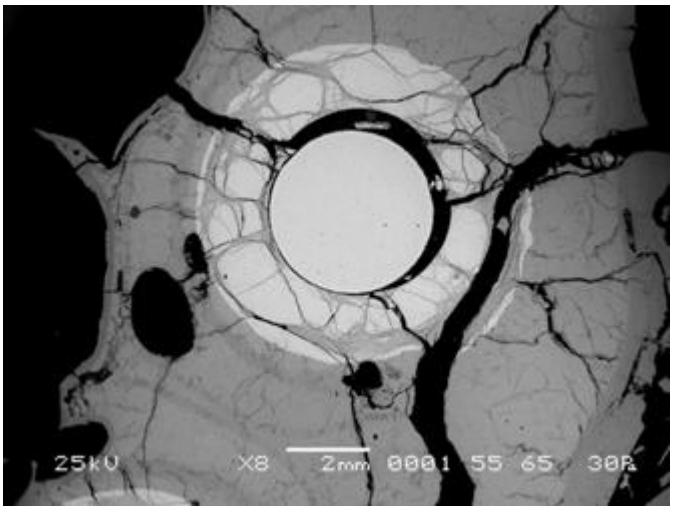

Rod 3.5

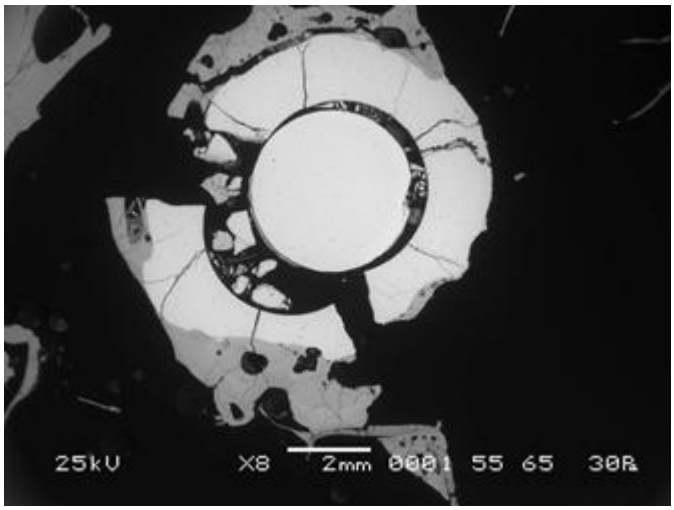

Rod 3.12

Рис. 30. Микроструктура поперечного сечения 793 мм модельной сборки PARAMETER–SF1.

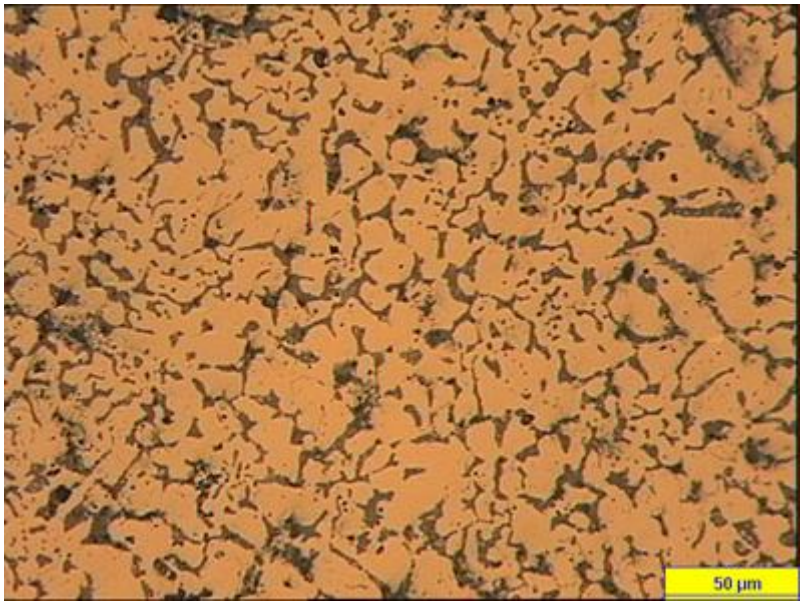

Zone A

Melt (U,Zr,O)
Ceramic faze content
~ 34 % vol.

Chemical compositions,
weight %.
Zr - **74.1**
U - **12.4**
Fe - **0**
Cr - **0**
Ni - **0**
O – **13.5**

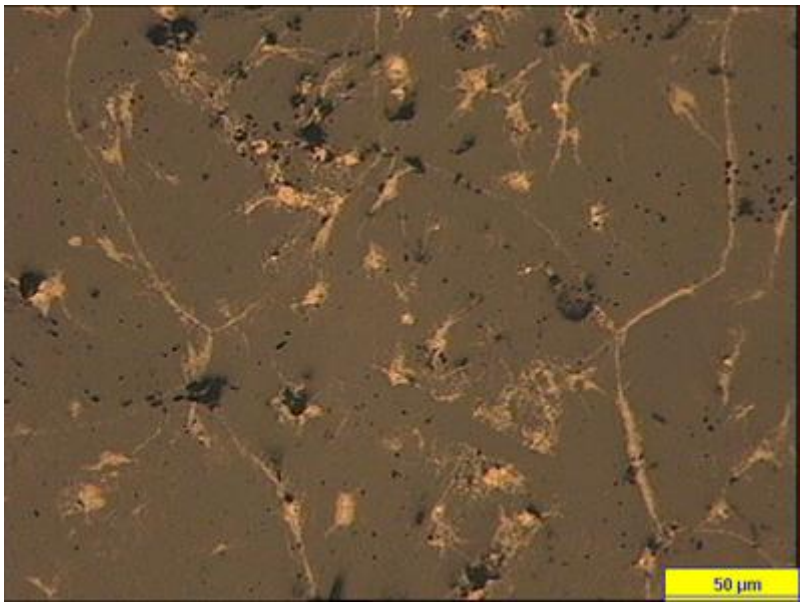

Zone B

Ceramic $(Zr,U)O_2$

Chemical composition,
weight %.

Zr - **58.6**
U - **15.2**
Fe - **0**
Cr - **0**
Ni - **0**
O – **25.9**
Ta - **0.3**

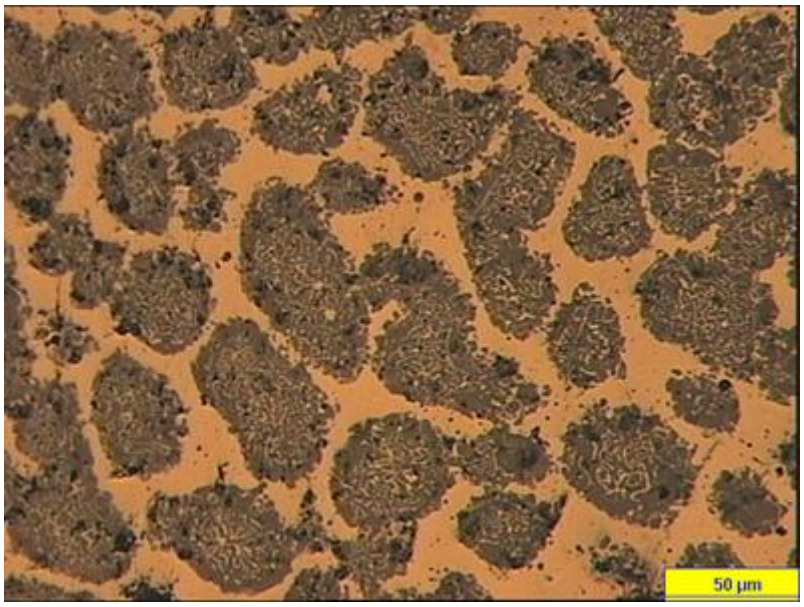

Zone C

Melt (U,Zr,O)
Ceramic faze content
~ 64 % vol.

Chemical composition,
weight %.

Zr – **61.1**
U - **18.2**
Fe – **0.2**
Cr - **0**
Ni – **0.1**
O – **19.0**
Ta - **1.3**

Fig. 31. Structures of melts from different zones of section 793 mm.

Fig. 32. Cross-section of the assembly at the level of 839 mm (top view).

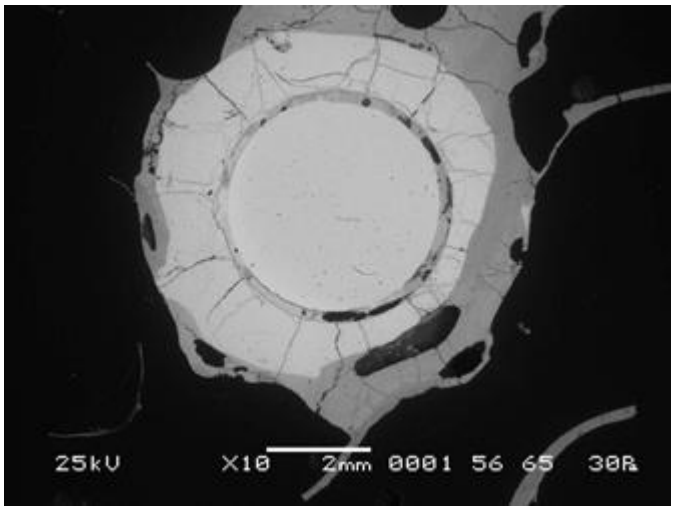

Rod 3.9.

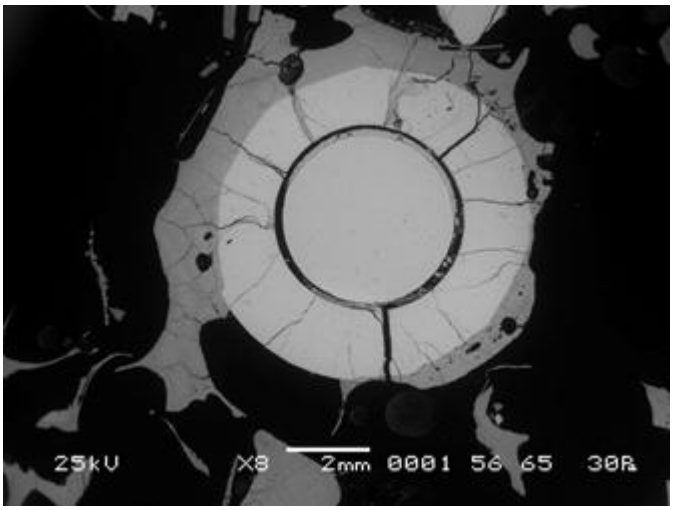

Rod 3.12

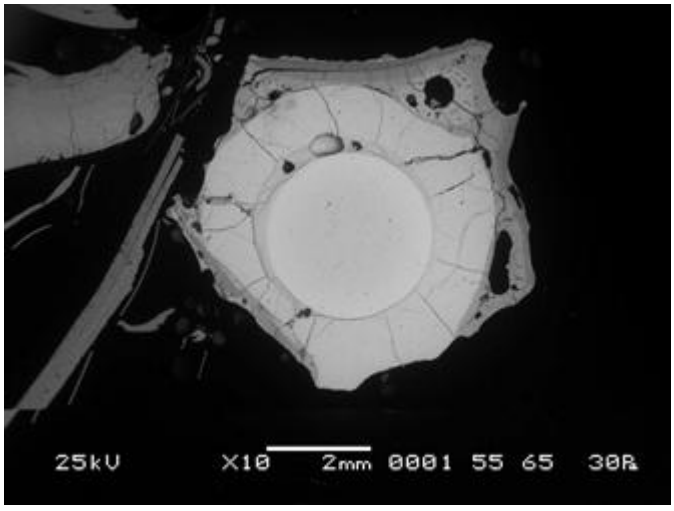

Rod 3.7

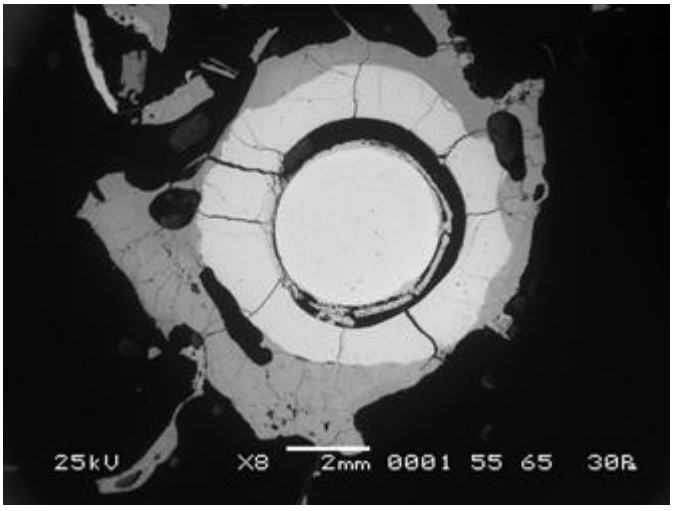

Rod 3.4

Fig. 33. Microstructure of cross-section 839 mm of the model assembly PARAMETER–SF1.

Fig. 34. Cross-section of the assembly at the level of 886 mm (top view).

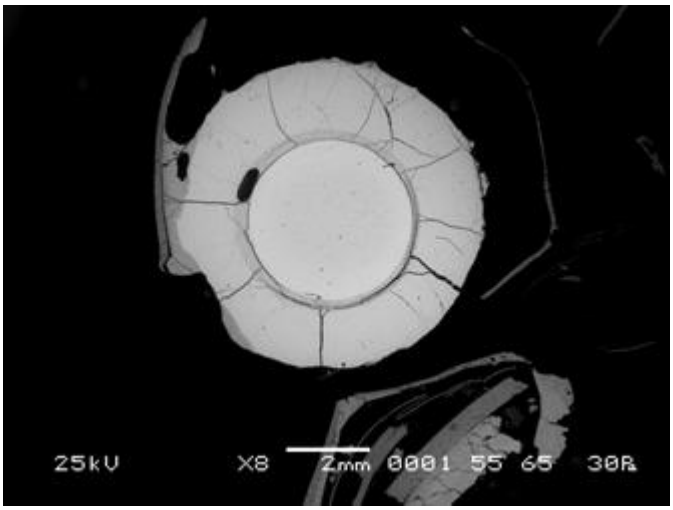

Rod 3.2

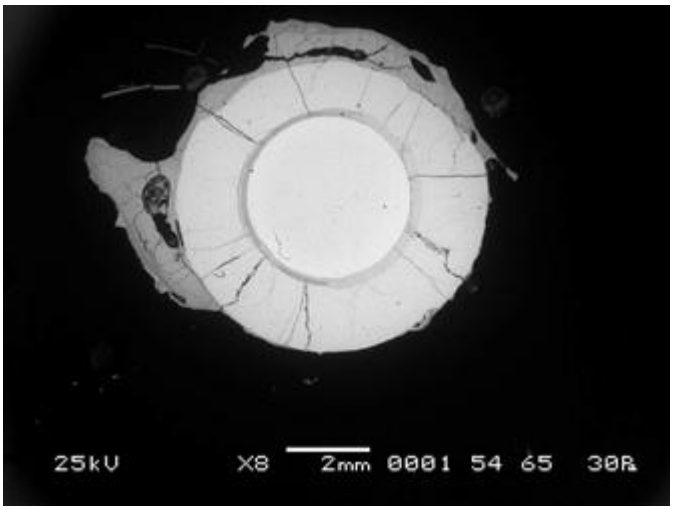

Rod 3.8

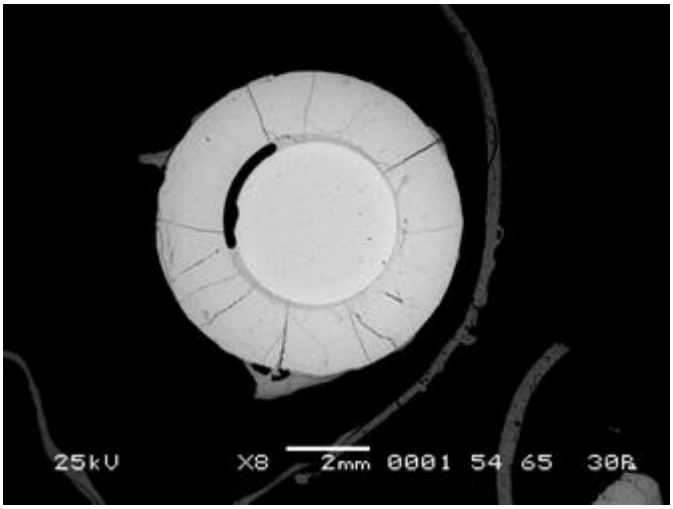

Rod 3.10

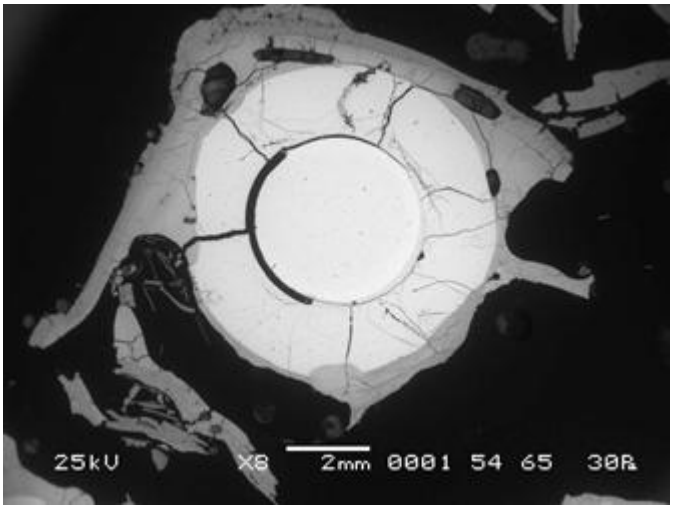

Rod 2.5

Fig. 35. Microstructure of cross-section 886 mm of the model assembly PARAMETER–SF1.

Fig. 36. Cross-section of the assembly at the level of 930 mm (top view).

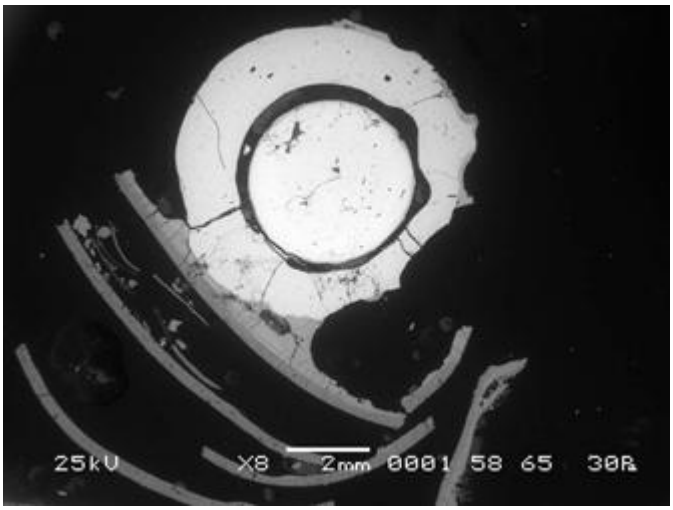

Rod 2.1

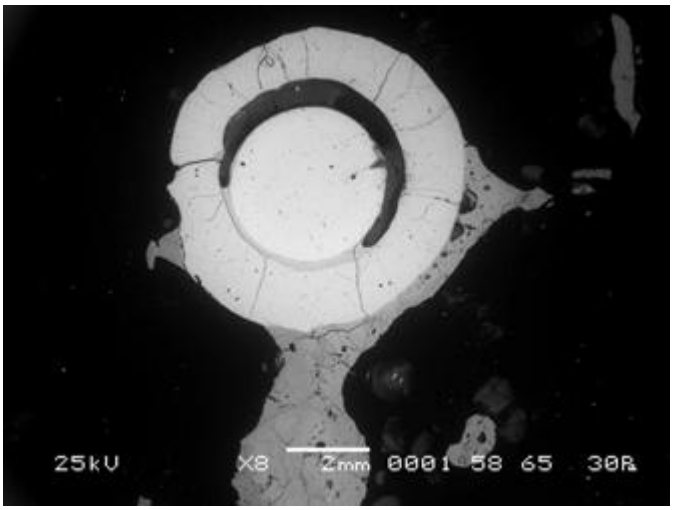

Rod 2.2.

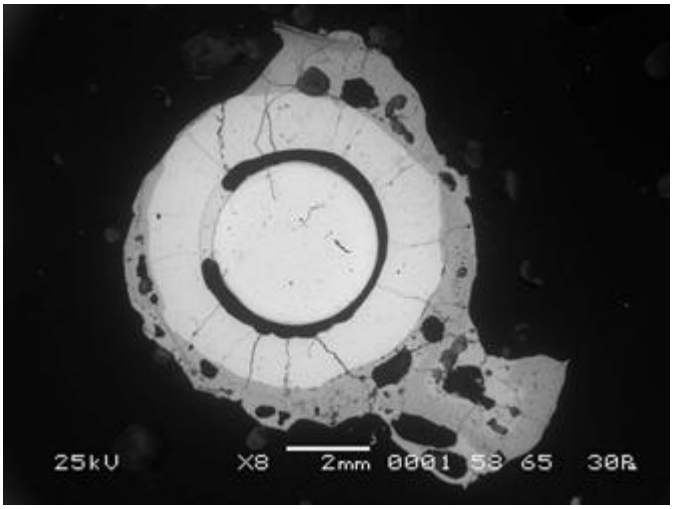

Rod 3.8.

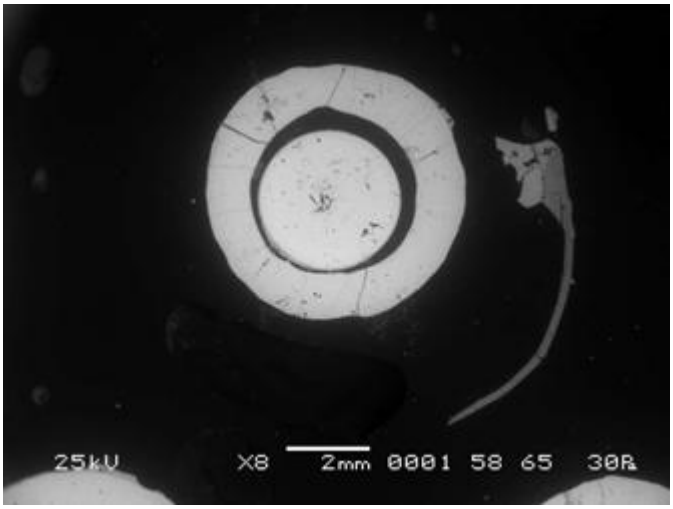

Rod 3.2

Fig. 37. Microstructure of cross-section 930 mm of the model assembly PARAMETER–SF1.

Fig. 38. Cross-section of the assembly at the level of 976 mm (top view).

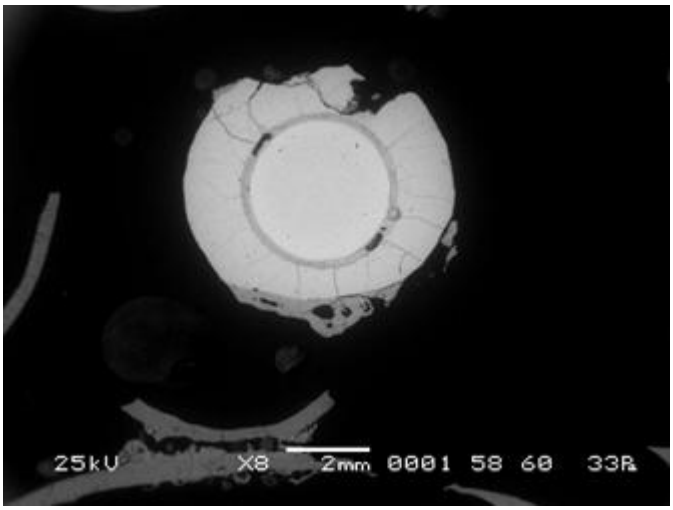

Rod 2.2

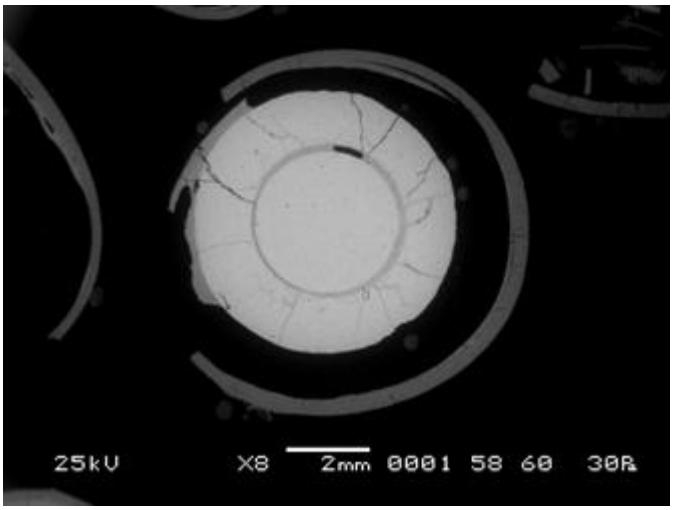

Rod 2.6

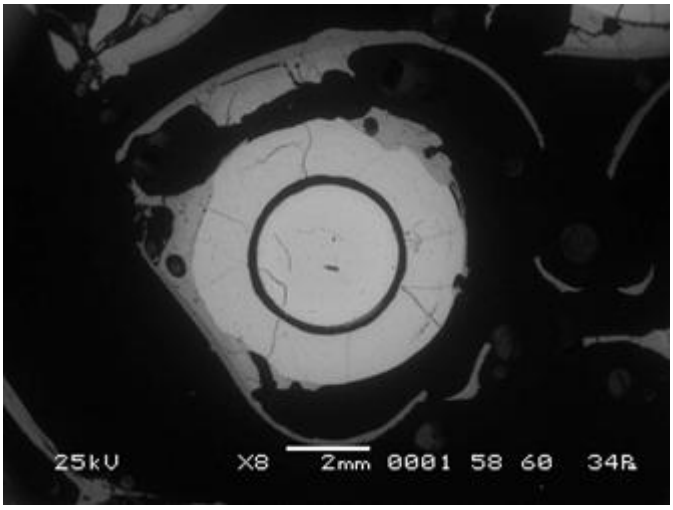

Rod 3.9

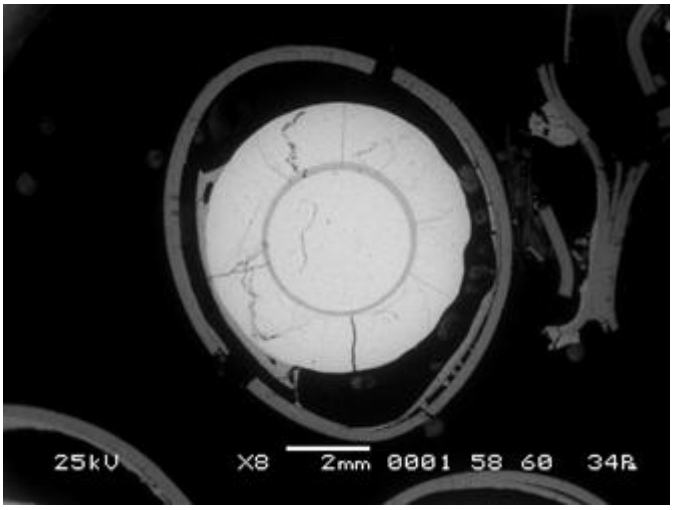

Rod 3.12

Fig. 39. Microstructure of cross-section 976 mm of the model assembly PARAMETER–SF1.

Fig. 40. Cross-section of the assembly at the level of 1021 mm (top view).

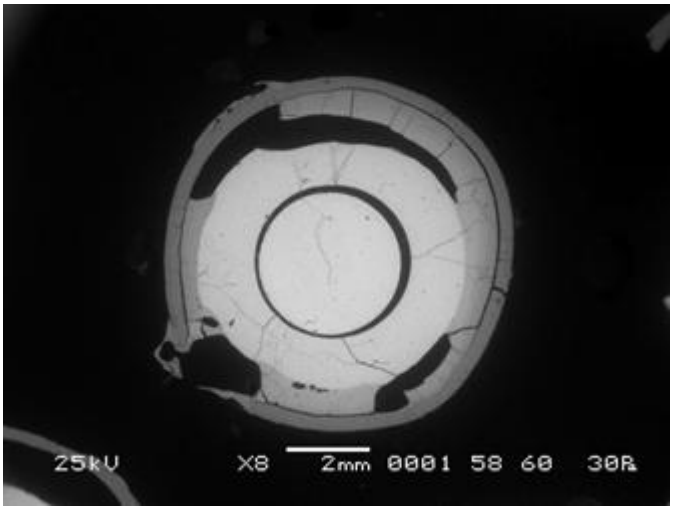

Rod 2.4

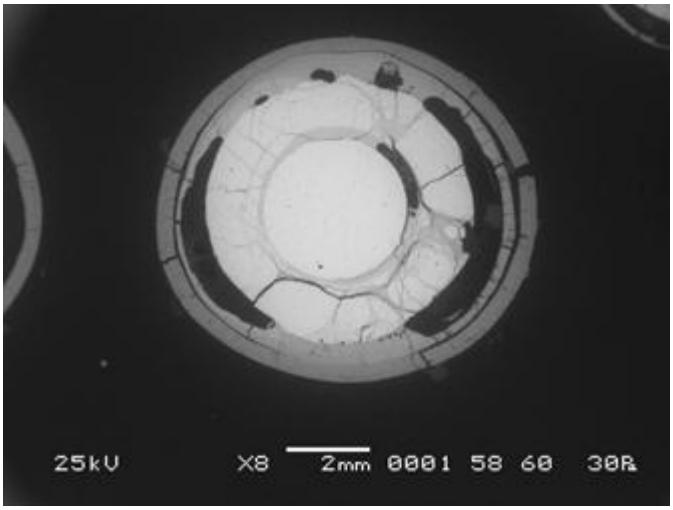

Rod 2.6

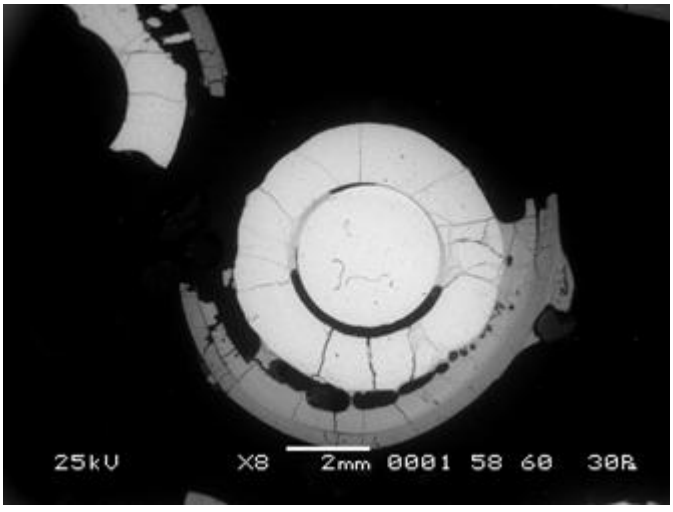

Rod 3.2

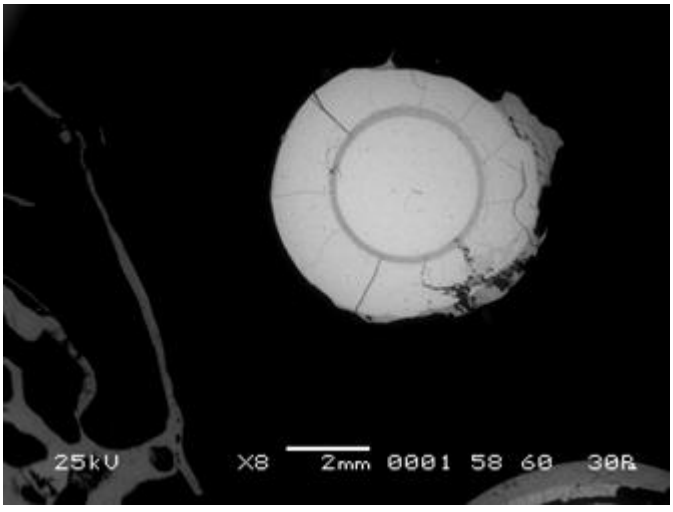

Rod 3.10

Fig. 41. Microstructure of cross-section 1021 mm of the model assembly PARAMETER–SF1.

Fig. 42. Cross-section of the assembly at the level of 1066 mm (top view).

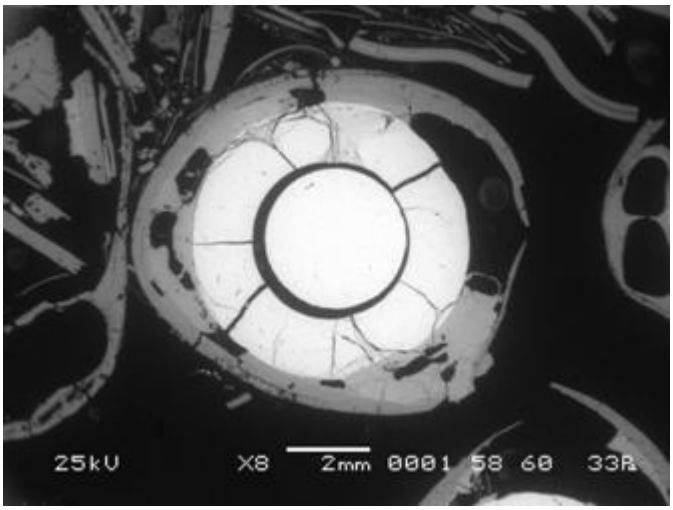

Rod 2.3

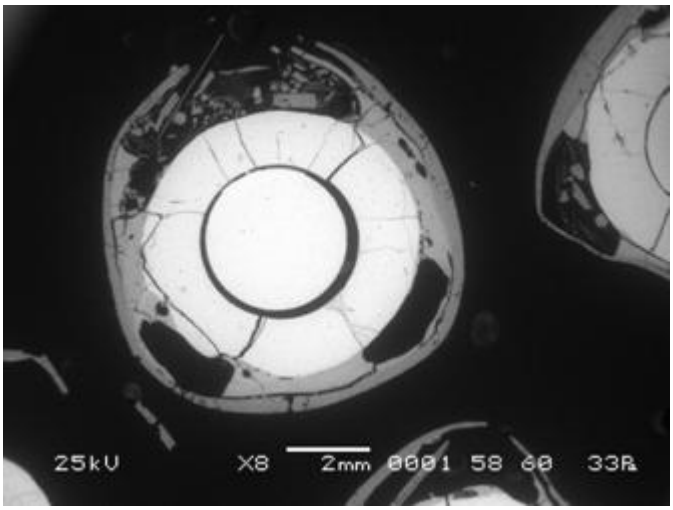

Rod 2.4

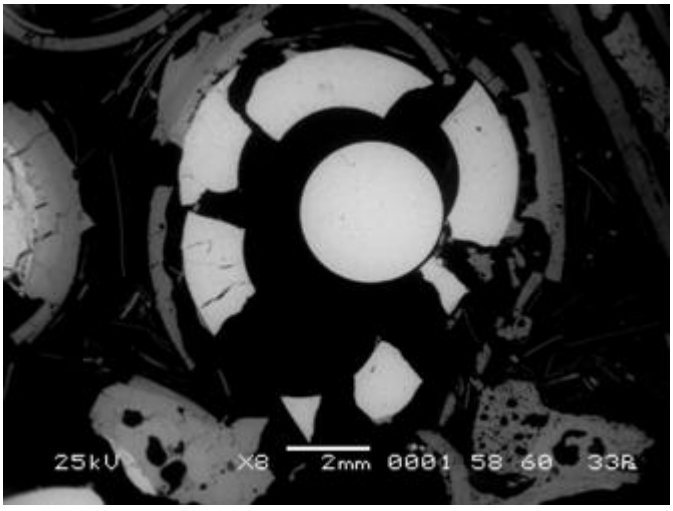

Rod 3.3

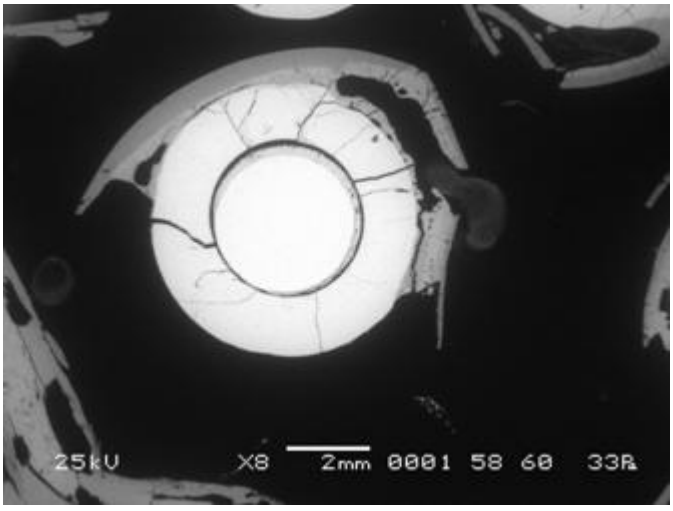

Rod 3.9

Fig. 43. Microstructure of cross-section 1066 mm of the model assembly PARAMETER–SF1.

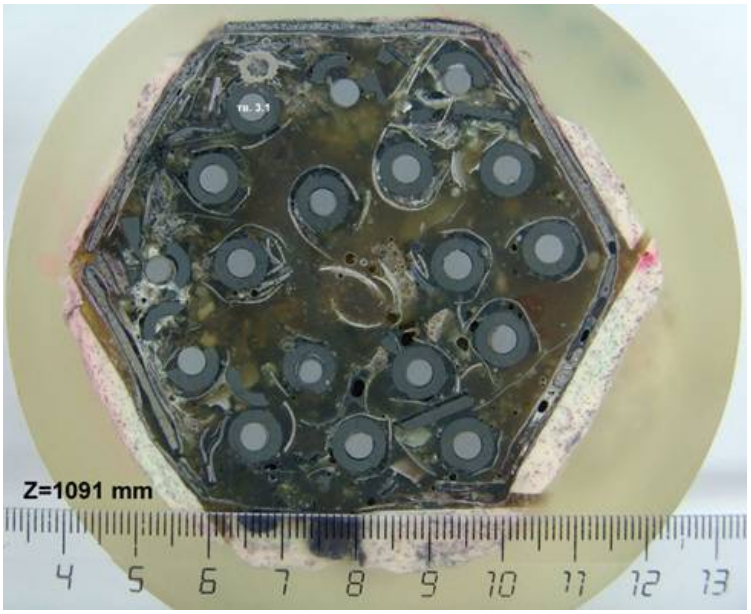

Fig. 44. Cross-section of the assembly at the level of 1091 mm (top view).

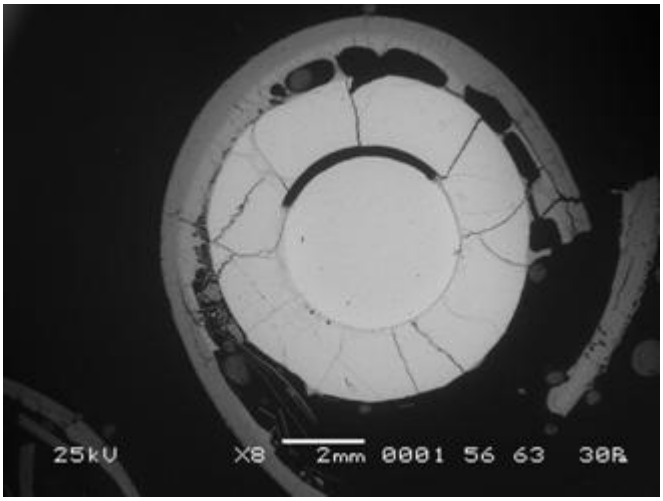

Rod 2.1

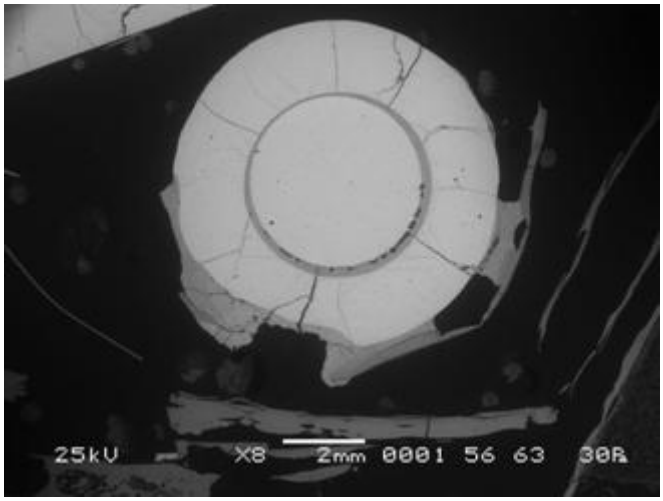

Rod 3.7

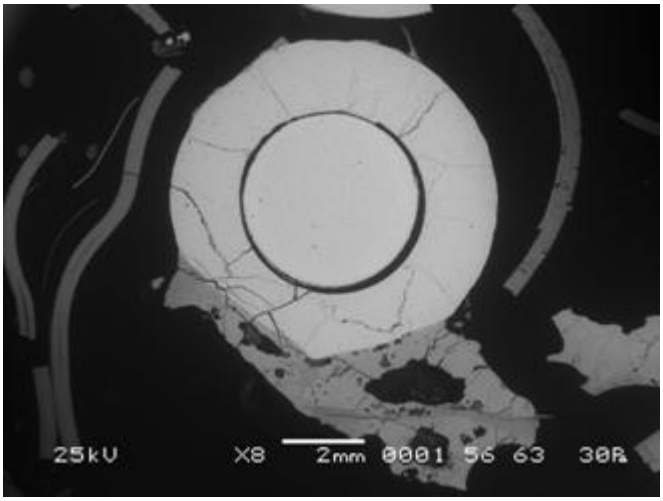

Rod 3.9

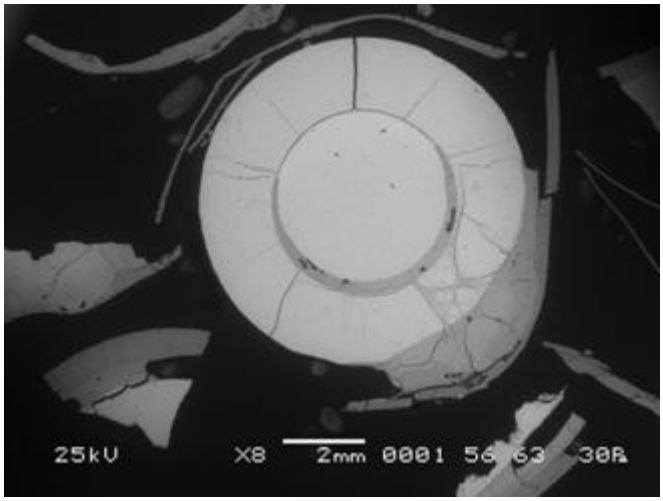

Rod 3.8

Fig. 45. Microstructure of cross-section 1091 mm of the model assembly PARAMETER–SF1.

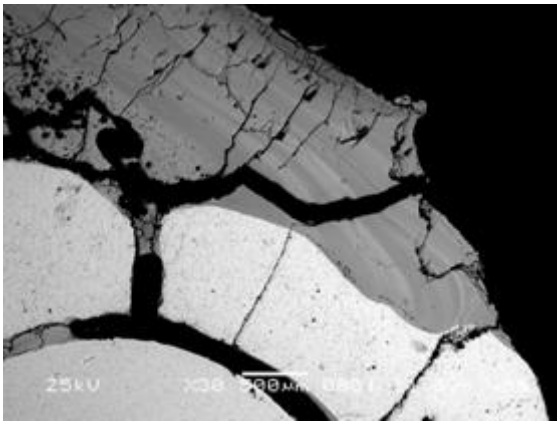

Z = 839 mm, Rod 2.4

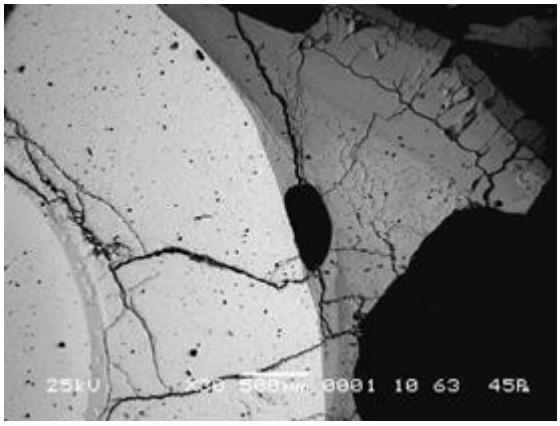

Z = 886 mm, Rod 2.5

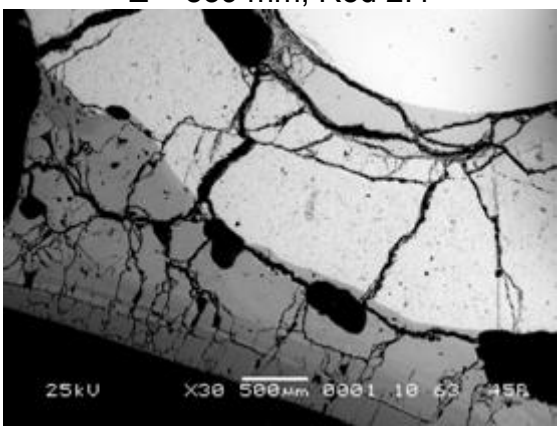

Z = 930 mm, Rod 2.3

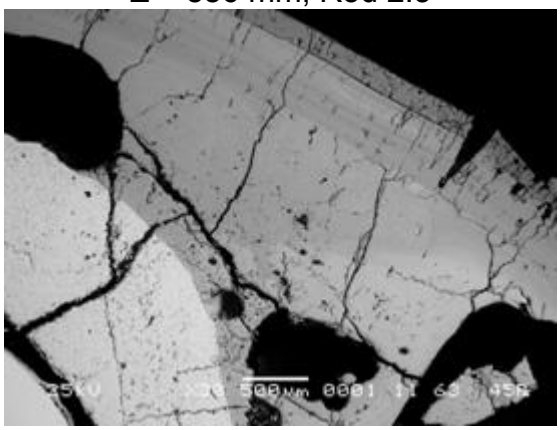

Z = 930 mm, Rod 2.5

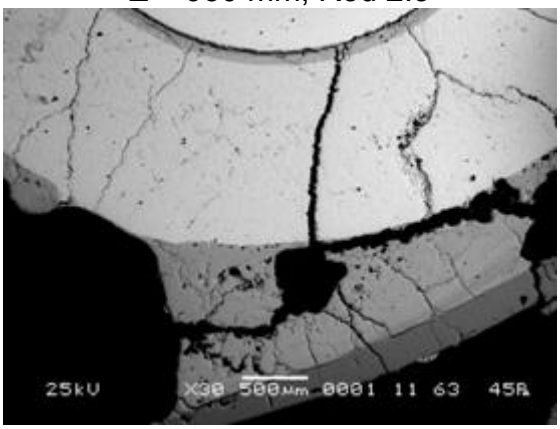

Z = 976 mm, Rod 2.5

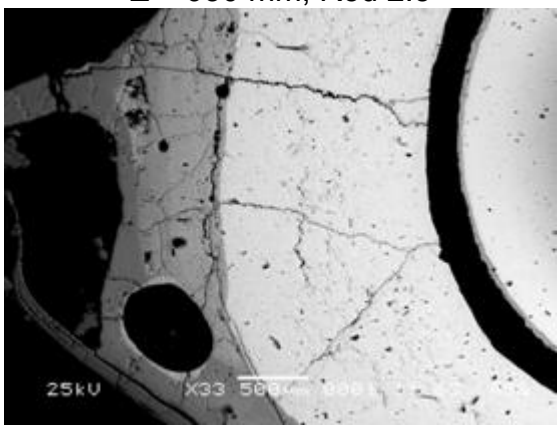

Z = 976 mm, Rod 3.9

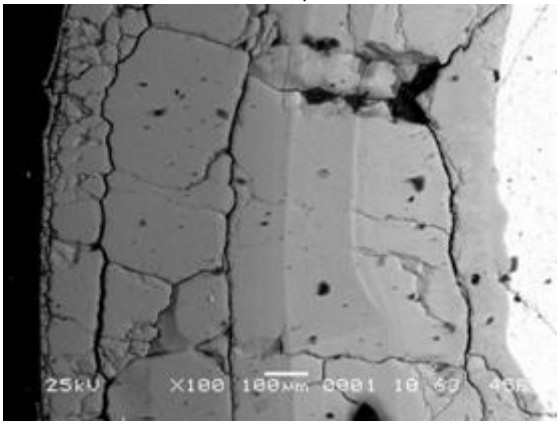

Z = 1021 mm, Rod 2.1

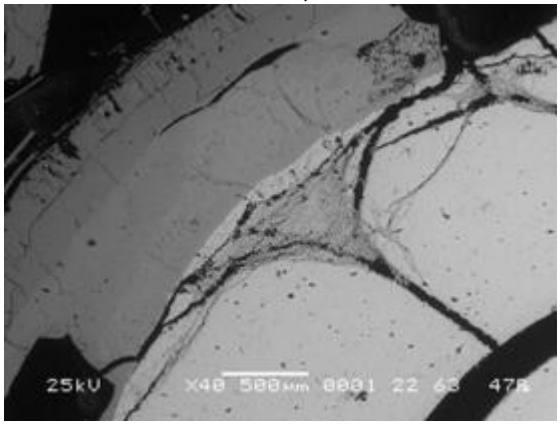

Z = 1066 mm, Rod 2.3

Fig. 46. Typical melt structures on fuel pellets within the elevation range Z = 800…1100 mm.

Fig. 47. Cross-section of the assembly at the level of 1156 mm (top view).

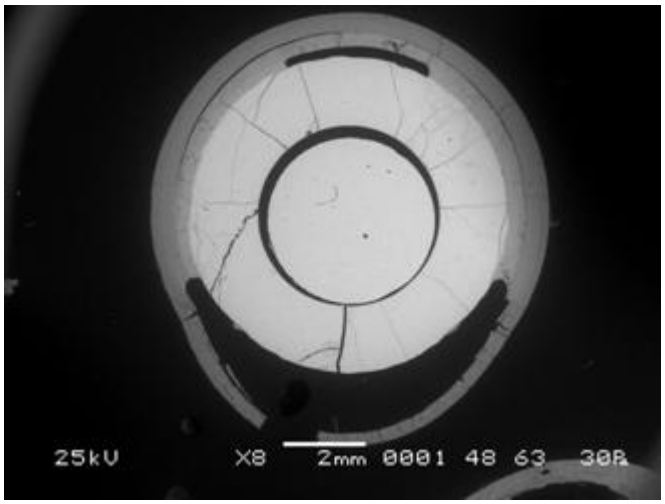

Rod 2.1

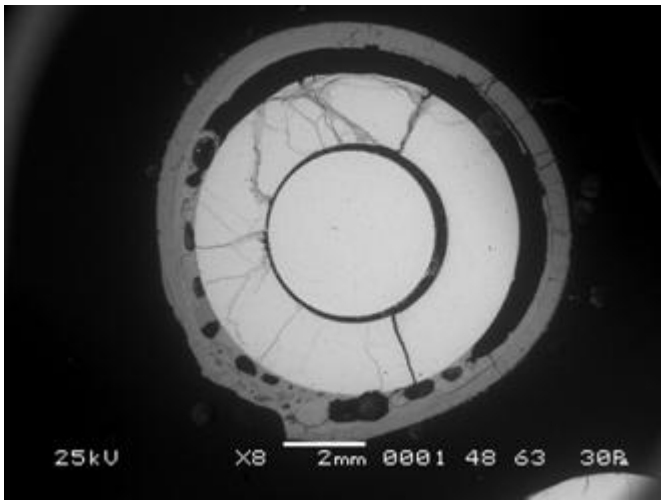

Rod 2.3

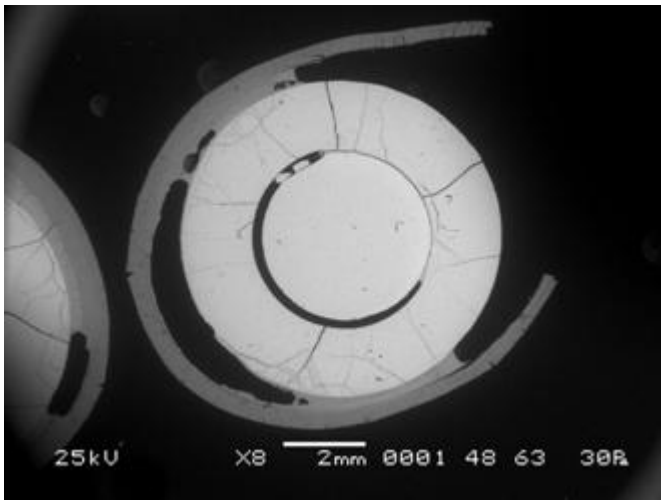

Rod 2.6

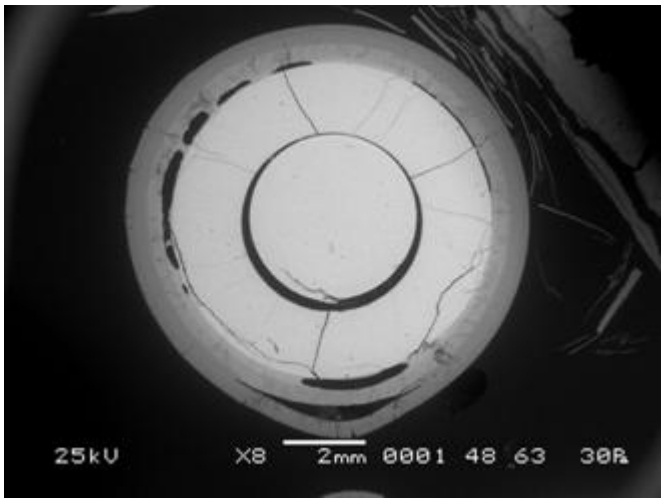

Rod 3.3

Fig. 48. Microstructure of cross-section 1156 mm of the model assembly PARAMETER–SF1.

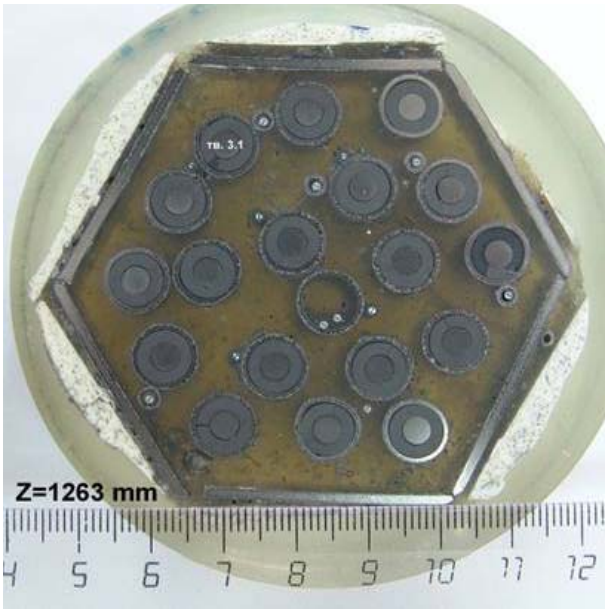

Fig. 49. Cross-section of the assembly at the level of 1263 mm (top view).

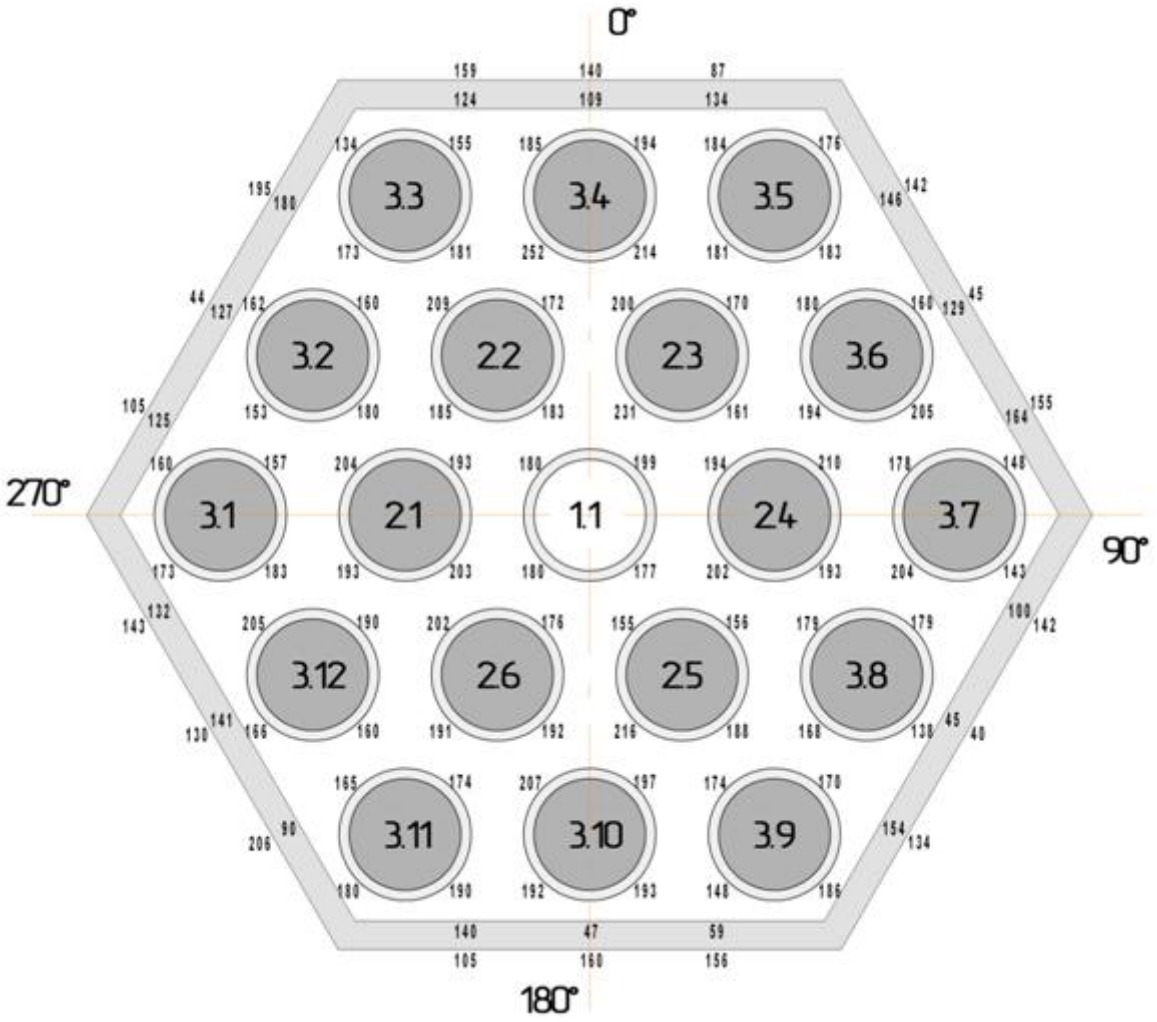

Fig. 50. Thickness of oxide layer on the surface of housing and shrouds at the level of 1263 mm.

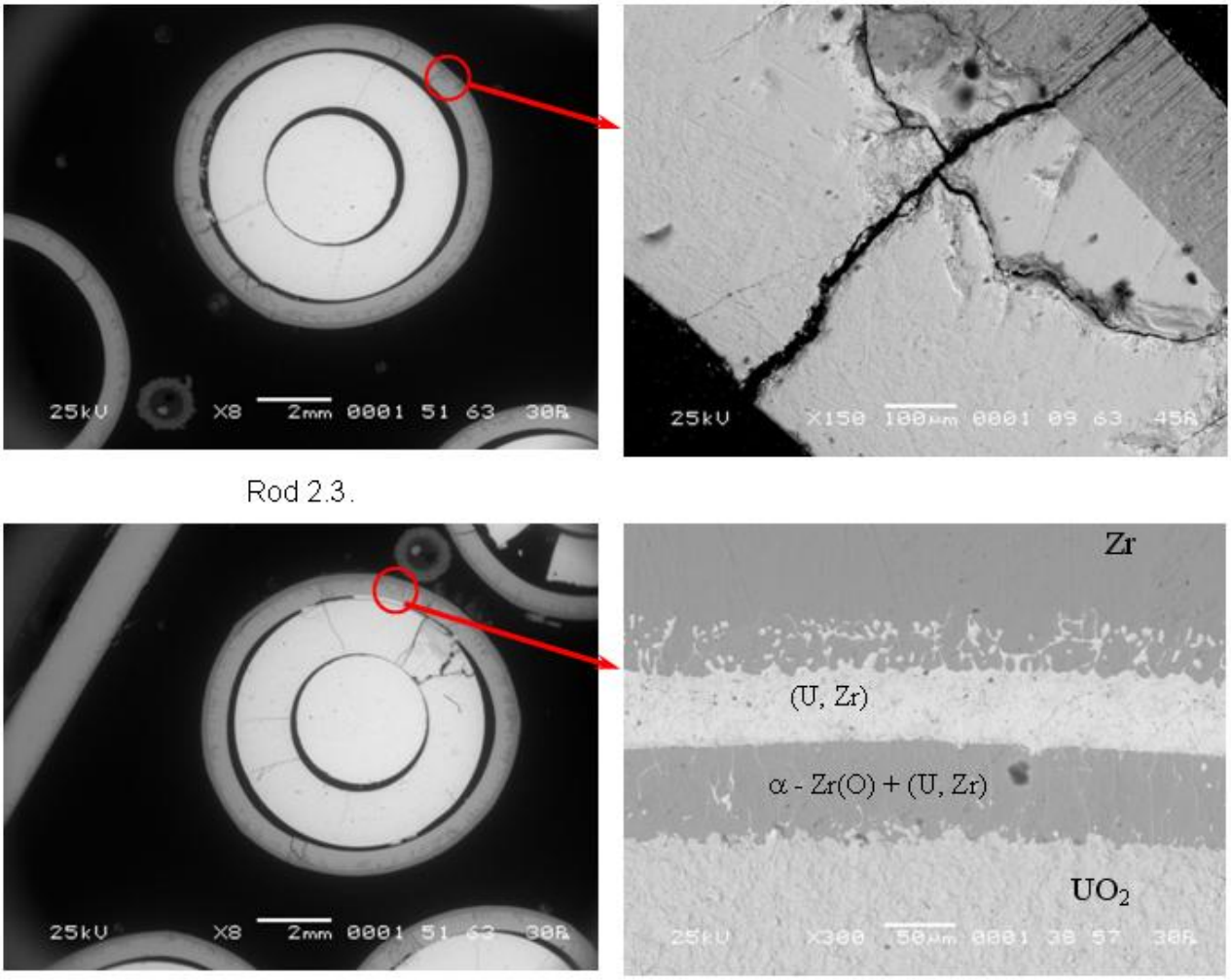

Fig. 51. Microstructure of cross-section 1263 mm
of the model assembly PARAMETER–SF1.

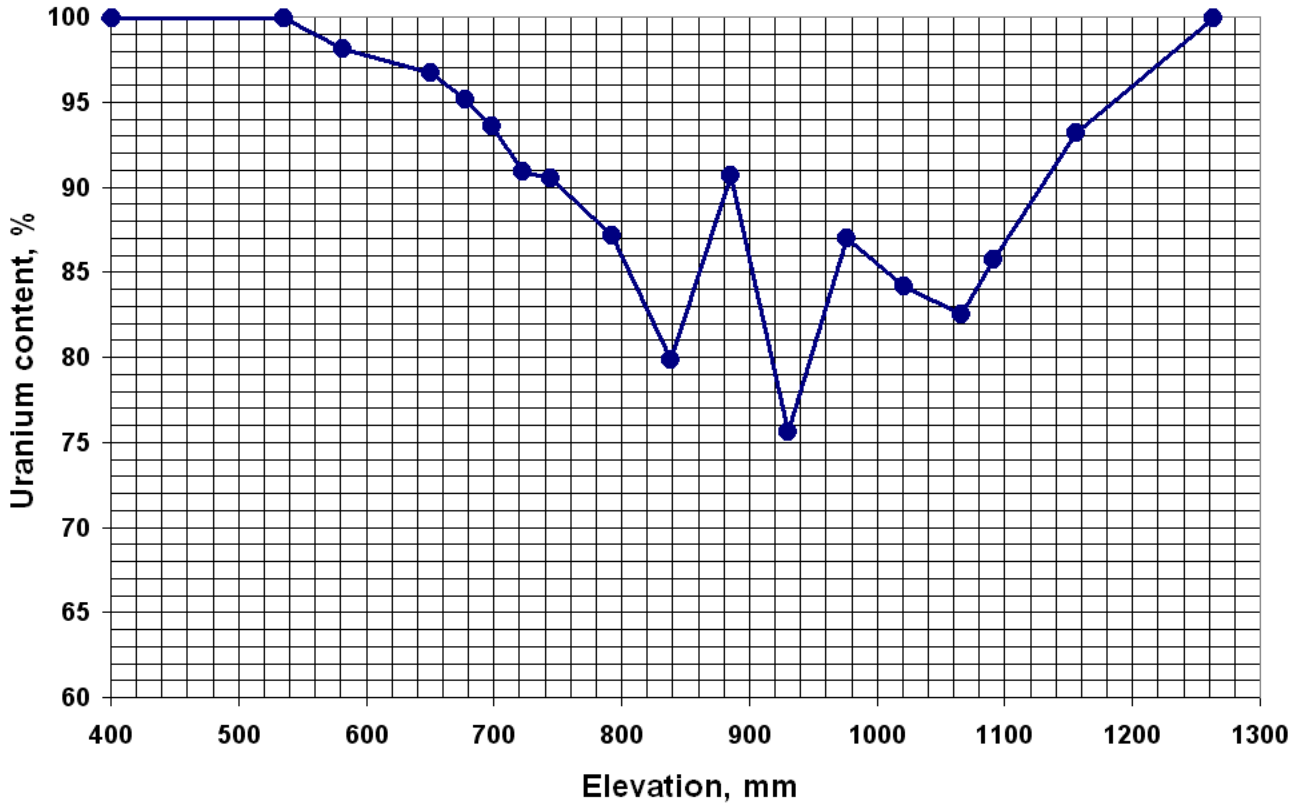

Fig. 52. Profile of the fuel dissolution in the model assembly PARAMETER–SF1.

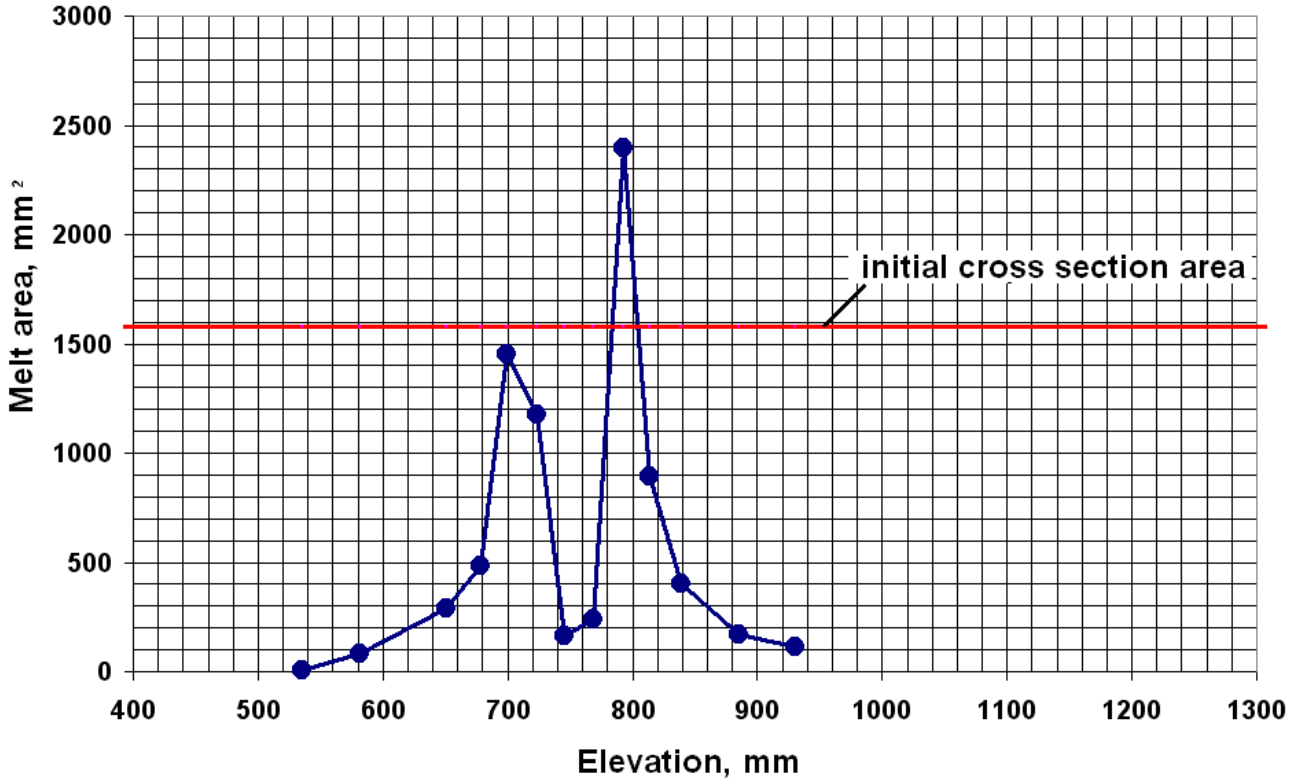

Fig. 53. Profile of the melt solidified in the model assembly PARAMETER–SF1.

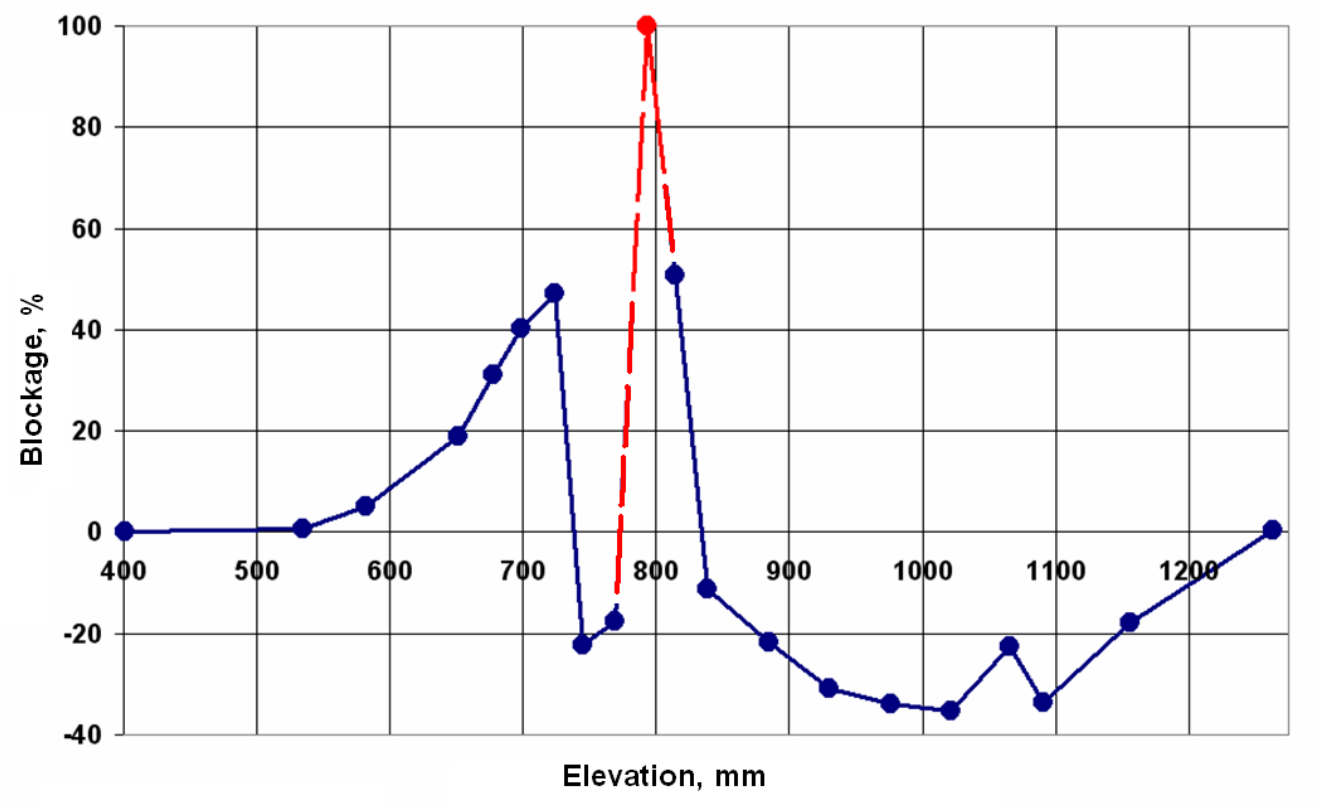

Fig. 54. Distribution of flow area blockage in the model assembly PARAMETER–SF1.

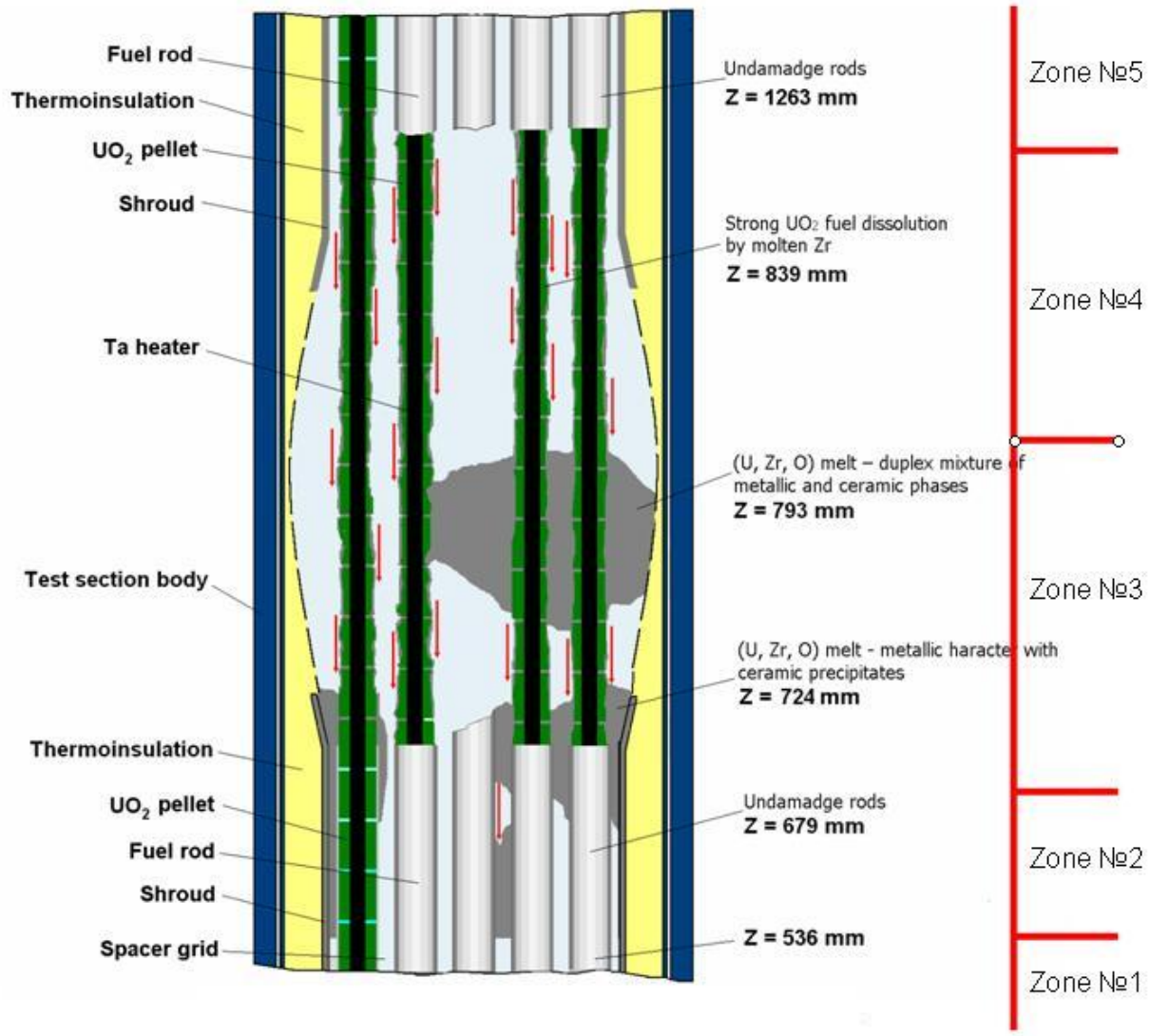

Fig. 55. Block diagram of the assembly after the tests.